Research article

Dynamical behavior analysis of the heart system by the bifurcation structures

R.F. Fonkou [a,b,c,*], Romanic Kengne [a], Herton Carel Fotsing Kamgang [a], P.K. Talla [c]

[a] Condensed Matter, Electronics and Signal Processing Research Unit, University of Dschang, B.P. 67, Dschang, Cameroon
[b] Laboratoire de Physique et Sciences de l'ingénieur, Institut Universitaire de la Côte, S/c BP 3001, Douala, Cameroon
[c] UR de Mécanique et de Modélisation des Systèmes Physiques (UR-2MSP), UFR/DSST, Université de Dschang, BP 67, Dschang, Cameroon

ABSTRACT

The functioning of the heart rhythm can exhibit a wide variety of dynamic behaviours under certain conditions. In the case of rhythm disorders or cardiac arrhythmias, the natural rhythm of the heart is usually involved in the sinoatrial node, the atrioventricular node, the atria of the carotid sinus, etc. The study of heart related disorders requires an important analysis of its rhythm because the regularity of cardiac activity is conditioned by a large number of factors. The cardiac system is made up of a combination of nodes ranging from the sinus node, the atrioventricular node to its Purkinje bundles, which interact with each other via communicative aspects. Due to the nature of their respective dynamics, the above are treated as self-oscillating elements and modelled by nonlinear oscillators. By modelling the cardiac conduction system as a model of three nonlinear oscillators coupled by delayed connections and subjected to external stimuli depicting the behavior of a pacemaker, its dynamic behavior is studied in this paper by nonlinear analysis tools. From an electrocardiogram (ECG) assessment, the heart rhythm reveals normal and pathological rhythms. Three forms of ventricular fibrillation, ventricular flutter, ventricular tachycardia and atrial fibrillation are observed. The results are confirmed by the respective maximum Lyapunov exponents. Considering the cardiac nodes as microchips, using microcontroller simulation technology, the cardiac conduction system was modelled as a network of four ATmega 328P microcontrollers. A similarity with the results obtained numerically can be observed.

1. Introduction

The regularity or irregularity of the heart rhythm is usually studied by analyzing the conduction systems of the heart [1–3]. The heart is considered as the central element of the cardiac conduction system [4-6]. The functioning of the heart requires an enormous need of oxygen. This oxygen allows the good regularity of the cardiac system because the latter has need to produce its own electricity. The information that our brain sends to it allows it to know what the body needs. Once it has received this information, to adapt its frequency to meet the needs of the body, it initiates the electrical impulse which evolves with a frequency adapted to the needs of the body [7,8]. To model the heart system three main nodes among the six heart nodes are considered, namely the sinus node (SA node), the atrioventricular node (AV node) and the Purkinje fibres (PF node) [9,10].

---

* Corresponding author.
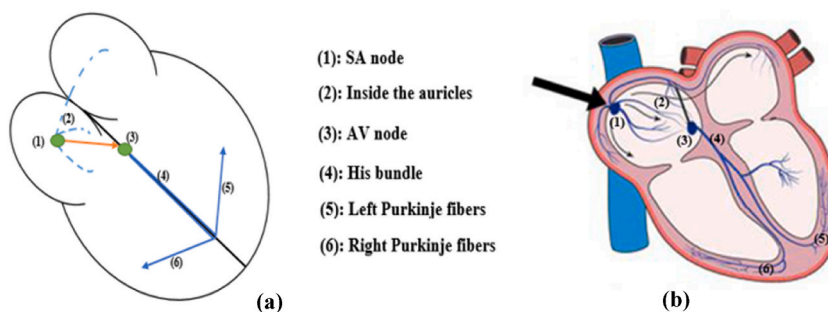 E-mail address: fonkourodrigue99@yahoo.com (R.F. Fonkou).

Fig. 1. (a) Diagram describing the functioning of the heart system; (b) Image of a real heart giving better clarity.
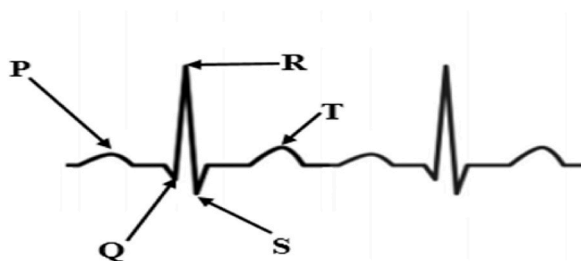

Fig. 2. ECG signal characterizing normal electrical activity.

The configuration of the heart presents a structure of four cavities, two atria, namely the right and left atria, and two ventricles, one on the left and one on the right. The electricity initiated for the functioning of the organism makes contract the two atria and the two ventricles. By crossing the atria and from the atrioventricular node, the electrical impulse created allows the blood to pass to the ventricles. In the ventricles, the electrical current also causes the contractions of the ventricles, allowing the blood to be propelled to the lungs by the right ventricle and into the whole body by the left ventricle [11-14]. Thus the electrical impulse travels through the body. The diagram describing the mechanism of operation of the cardiac system is given in Fig. 1a and b.

The heart rhythm is governed by the flow of this impulse as it passes through the heart and allows all the structures of the heart to contract synchronously. This is the regulatory core of the heart rhythm [15,16]. In the cardiac system, the node of origin of the electrical impulse is the sinus node, also known as the natural pacemaker. This node is located in the atria in the upper part of the right atrium. This rhythm imposed by the sinus node is regulated by various factors: the nervous system, hormones and substances circulating in the blood. However, a large number of disturbances can occur, which can affect the sinus node, the AV node, the atria and the ventricles, resulting in the loss of synchronization of the cardiac structures [17-20]. Cardiac rhythm is characterised by variations in the electrical potential of cells, some of which promote contraction and others automation and impulse conduction [7, 21]. One of the best interpretations of these different behaviours of the electrical activity of the heart is the analysis of the electrocardiogram signal [22-25].

The electrocardiogram (ECG) is the graphic representation of the electrical activity of the heart. It is presented in the form of a paper trace whose curve may, during normal heart function, show the five main waves, namely the P wave, the QRS complex and the T wave as shown in Fig. 2 [26-28]; JiQian [29]. In normal electrical activity, contraction and depolarization of the atria are caused by the P wave. Its period varies from 0.08 to 0.1 s, its amplitude is less than 2 mm. The depolarization and contraction of the ventricles are due to the QRS complex. The first negative wave of the complex is Q, the first positive wave is R and the second negative wave is S. Between the onset of the P wave and the QRS complex, the period varies from 0.12 to 0.20 s. This time corresponds to the PR or PQ interval and represents the time taken for the electrical impulse to travel from the sinus node through the atria to the ventricles. In the presence of an elevated rhythm, there is a decrease in the PR interval. The transition between the QRS complex and the ST segment is called the J point. The period corresponding to the QRS complex and the beginning of the T wave is the ST segment.

With the ECG signal, the electrical activity is measured and the functioning of the heart can be analyzed. Each wave of the ECG signal causes the heart muscle to contract, which promotes blood flow. However, seeing the ECG signal in its normal form does not mean that the heart is healthy, as the form of an abnormal ECG can also be insignificant. Only in the option of confirming a diagnosis does the doctor use the ECG to support his or her assumptions. The ECG provides an easy way to analyse the rhythm and heart rate (number of QRS per unit of time). In the normal state, a constant R-R space is observed, the formation of the P wave before each QRS

complex, which in turn must appear before each T wave. A PR interval must also be observed.

In the presence of disturbances, an increase or decrease in rhythm leading to arrhythmias can be observed depending on the degree of activity [30-33]. These disturbances sometimes occur for no apparent reason. Cardiac rhythm disorders are frequent pathologies. Their number is constantly increasing due to the ageing of the population and improved detection methods. In order to study cardiac activity through its dynamics, researchers have modelled the conduction system of the heart as a network of self-oscillating elements modelled by nonlinear oscillators [34]; Aino-Maija [35-39]. The first oscillator modelling cardiac activity being the Van der Pol oscillator [23,40], in order to reduce the high order of the equations the modelling of the heart has been done by a large number of oscillators [41,42]. They propose a more appropriate description of the natural pacemaker and are reduced versions of the Van der Pol oscillator, including the Hodgkin-Huxley model [43], the FitzHugh and Nagumo model [44], the Grudzinsky-Zebrowsky model [45]. Based on these oscillators, a large number of works on the heart in its perturbed state have been carried out. This is the case of Fonkou et al. [46,47]. Let us also note the work of Krstacić et al. [48], Ernst and Bar-Joseph [49], Tobon et al. [50], Shiraishi et al. [51], Savi [52]. To analyse the heart rate, these researchers have proposed a large number of methods. In reference [53], Savi and Gois propose an analysis of heart rate by a random selection of parameters. In Ref. [2], Cheffer and Savi also use a random choice of parameters to study electrical activity, in the same work by plotting Poincaré sections they confirm the results obtained. Fonkou et al. study in Ref. [41] the dynamic behavior of the heart by nonlinear analyses only on the sinus node. In the same logic, Kuate and Fotsin [54] analyse the rhythm by an experimental study based on electronic components.

In the present work, in order to analyse and interpret the physiological behavior of the cardiac rhythm, a study of the dynamic behavior of the cardiac system is proposed. Using nonlinear analysis tools, essential ECG features illustrating normal and pathological physiologies are captured. Two contributions emerge from this work. The first is to use as bifurcation parameters, the coupling parameters indicating communication aspects, the amplitude of external stimuli and the AV node parameter in order to highlight through the evaluation of the electrocardiogram (ECG) the values of the parameters for which the heart rhythm is normal or pathological. These results obtained are confirmed by the maximum Lyapunov exponents corresponding to each bifurcation curve. Considering the cardiac nodes as electronic chips, the second one consists in using an experimental study by real implementation with the ATmega 328P microcontroller to model the heart as a network of four microcontrollers each representing a cardiac node. The results obtained show a good qualitative agreement with the numerical results.

The rest of the work is structured as follows: the mathematical modelling of the cardiac system is given in section 2. The presentation of the ECG signal in section 3. Section 4 presents the results obtained by the nonlinear computational tools/approaches. The results obtained by a real implementation with microcontrollers are given in section 5. The work ends with a conclusion in section 6.

2. Mathematical modelling of the heart system

The constant propulsion of blood through the body is conditioned by the regularity of the heart rhythm. The heart is a reddish-brown, closed-dot muscle consisting of the right and left heart. It is composed of nodes such as the SA node, the AV node, and the Purkinje bundles. To cause the heart chambers to contract, electricity flows through the heart. This electricity is created by the Keith and Flack node (SA node), also known as the natural pacemaker, which is located in the upper right chamber (atrium). To propel blood into the lower chambers (ventricles), the atria are synchronously contracted by the electrical impulse passing through them. Then, from the atrioventricular node (or AV node), the ventricles receive the electrical impulse and transmit it to the His bundle. Once the impulse reaches the bundle, it is directed to the left and right Purkinje fibres, causing the ventricles to contract, allowing the right to propel blood to the lungs and the left to the rest of the body. This is the circuit followed by the electrical impulse in the heart. Each of these paths leads to a heartbeat.

Each of these heartbeats is stimulated by electrical signals that follow a specific nerve pathway in the heart. These signals can be monitored and recorded by an electrocardiogram (ECG). The heart is usually associated with its conduction system because the latter constitutes the main nodes that characterize it. It functions as a pacemaker, maintaining between 60 and 100 beats per minute of heart activity. If the activity of this system is interrupted due to a heart injury or any other pathology, the heart rhythm is disturbed or irregular. In this case, blood flow to the brain and other parts of the body may be impaired. Recently, there has been a great deal of work on mathematical modelling of electrical activity [53,55,56]. In their work, researchers have developed a large number of mathematical and physical techniques, which have allowed them to model the heart rhythm more easily. They consider the cardiac system as a network of three nonlinear oscillators in which the communication aspects between the different oscillators are provided by coupling parameters or delayed connections. The rhythm disturbance is related to stimuli representing external pacemakers leading to an increase in the size of the system.

Based on the use of a nonlinear equation model of the heart rhythm in this work, the mathematical model of the heart is given by a coupled system of three nonlinear Grudzinsky-Zebrowsky type oscillators coupled by delayed connections. The system of differential equations given in equation (1) represents its dynamics.

$$\begin{cases} \dot{x}_1 = x_2 \\ \dot{x}_2 = F_1(t) - \alpha_1(x_1 - v_1)(x_1 - v_2)x_2 - \dfrac{\omega_{01}^2}{e_1 d_1}x_1(x_1 + d_1)(x_1 + e_1) + k_{1-3}(x_3(t - \tau_{1-3}) - x_1) \\ \qquad + k_{1-5}(x_5(t - \tau_{1-5}) - x_1) \\ \dot{x}_3 = x_4 \\ \dot{x}_4 = F_2(t) - \alpha_2(x_3 - v_3)(x_3 - v_4)x_4 - \dfrac{\omega_{02}^2}{e_2 d_2}x_2(x_3 + d_2)(x_3 + e_2) + k_{3-1}(x_1(t - \tau_{3-1}) - x_3) \\ \qquad + k_{3-5}(x_5(t - \tau_{3-5}) - x_3) \\ \dot{x}_5 = x_6 \\ \dot{x}_6 = F_3(t) - \alpha_3(x_5 - v_5)(x_5 - v_6)x_6 - \dfrac{\omega_{03}^2}{e_3 d_3}x_5(x_5 + d_3)(x_5 + e_3) + k_{5-3}(x_3(t - \tau_{5-3}) - x_5) \\ \qquad + k_{5-1}(x_1(t - \tau_{5-1}) - x_5) \end{cases} \qquad (1)$$

The one-way coupling coefficient allowing the node p to communicate with the node q is given by k_{q-p}. When the signal created by the node q arrives at the node p, this one filters the signal by imposing a delay to it τ_{q-p} to the needs of the organism in case of heart rhythm disturbances. The heart activity being most often disturbed, in this case, they are represented by $F_m(t) = \beta_m \sin(\omega_m t)$ and characterizes the external stimuli causing the increase in the size of the system. p, q or m can correspond as well to the SA node, the AV node or the Purkinje fibers.

3. ECG signal presentation

The graphic representation of cardiac activity is most often linked to a paper chart showing the variations in electrical potentials. This paper chart is called an electrocardiogram (ECG). It is usually used by the doctor to diagnose patients by determining whether their electrical activities are normal or irregular, as many heart problems can be determined from abnormal ECG results. In cardiology, the ECG is essential because it can be ordered in situations of chest pain to determine arrhythmias. It may also be recommended in the case of cardiac disorders to check for the presence of coronary insufficiency, cardiac dilatation. It is characterised by the presence of its five essential waves, namely the P, Q, R, S and T waves.

Depolarization of the atria is due to the P wave. Depolarization of the ventricles is due to the QRS complex. Its shape and amplitude are conditioned by variations in the heart muscle. The PQ or PR interval characterizes the duration between the onset of the P wave and the start of the QRS complex. In the normal state, also known as sinus rhythm, most QRS complexes are controlled by the P wave originating from the sinus node. The duration of this wave (P wave) is less than 0.12s and its amplitude is less than 0.25 mV. The P wave is positive in all leads except RV and V1. It is negative at VR and biphasic at V1. Between 0.12s and 0.20s, the PR space is isoelectric. For an onset time of the intrinsic deflection <0.04s, the QRS complex duration is less than 0.11.

From the combination of the three nodes of the system given in (1) i.e. the sinus node, the atrioventricular node, and the Purkinje fibers (PF), the ECG signal is constructed and its mathematical expression is given by equation (2)

$$X = \mu_1 x_1 + \mu_2 x_3 + \mu_3 x_5 \qquad (2)$$

Its differential equation is given in equation (3):

$$\dot{X} = \frac{dX}{dt} = \mu_1 x_2 + \mu_2 x_4 + \mu_3 x_6 \qquad (3)$$

With μ_1, μ_2, μ_3 constants. (x_1, x_2) describes the sinus node, (x_3, x_4) atrioventricular node and (x_5, x_6) Purkinje fibers. The values of the parameters α, v, d, e and ω_0 for each node are shown in Table 1. The external stimuli describing the pacemakers of each of the heart nodes are respectively: $F_1(t) = \beta_1 \sin(\omega_1 t)$ for the SA node, $F_2(t) = \beta_2 \sin(\omega_2 t)$ for the AV node and $F_3(t) = \beta_3 \sin(\omega_3 t)$ for Purkinje

Table 1
Parameters of the different nodes.

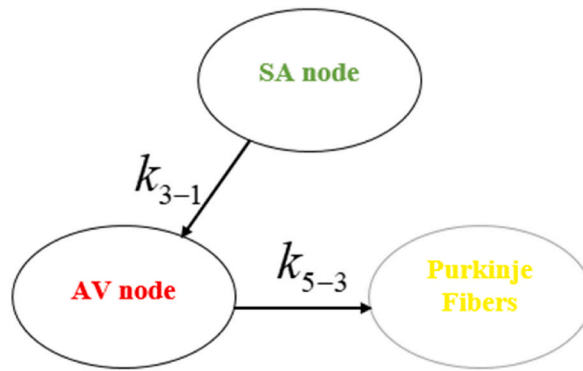| SA node	AV node	Purkinje Fibers
$\alpha_1 = 3.0$	$\alpha_2 = 3.0$	$\alpha_3 = 5.0$
$v_1 = 0.2$	$v_3 = 0.2$	$v_5 = 1.1$
$v_2 = -1.9$	$v_4 = -0.1$	$v_1 = -1.0$
$e_1 = 4.9$	$e_2 = 3.0$	$e_3 = 7.0$
$d_1 = 3.0$	$d_2 = 3.0$	$d_3 = 3.0$
$\tau_{1-3} = 0.0$	$\tau_{3-1} = 0.8$	$\tau_{5-1} = 0.0$
$\tau_{1-5} = 0.0$	$\tau_{3-5} = 0.0$	$\tau_{5-3} = 0.1$
$k_{1-3} = 0.0$	$k_{3-1} = 5.0$	$k_{1-5} = 0.0$
$k_{1-5} = 0.0$	$k_{3-5} = 0.0$	$k_{5-3} = 20.0$
$\omega_{03} = 4.583$	$\omega_{02} = 3.0$	$\omega_{03} = 4.583$

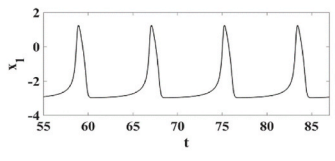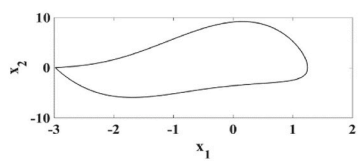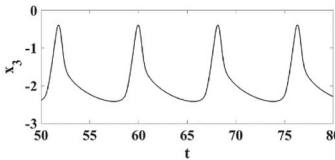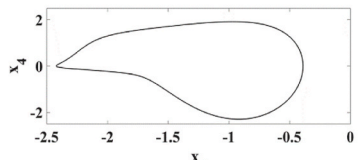**Fig. 3.** Conceptual diagram of the normal functioning of cardiac activity.

Heart nodes	Times traces	Phases portraits
SA node		
AV node		
Purkinje Fibers (PF)		
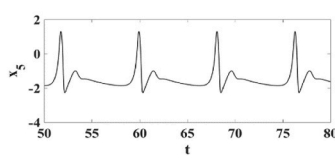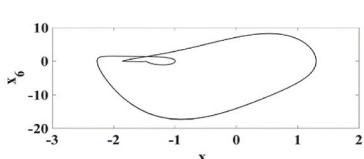
Fig. 4. Response of each oscillator obtained numerically with $x_{1,3,5} = 0.01$ et $x_{2,4,6} = 0.04$
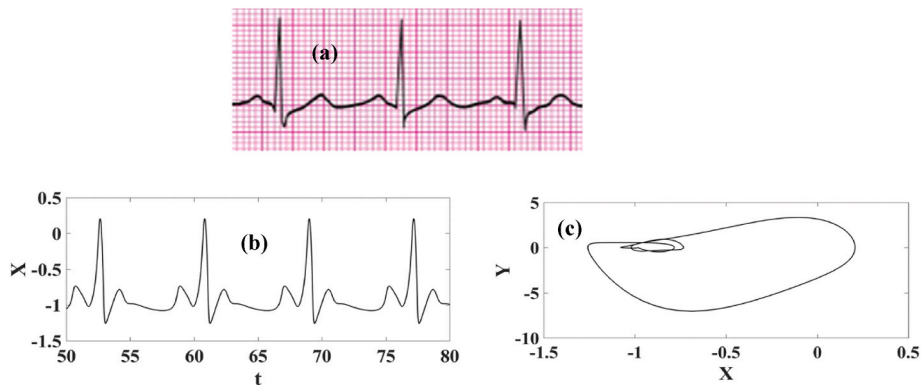

Fig. 5. (a) ECG signal obtained experimentally [57] and ECG signal obtained digitally: (b) time traces of ECG signal; (c) phase portrait of ECG signal with $x_{1,3,5} = 0.01$ et $x_{1,3,5} = 0.01$

fibres (PF).

For parameter values μ given by $\mu_1 = 0.1$, $\mu_2 = 0.05$ and $\mu_3 = 0.4$, using the Runge Kutta discretization method of order 4 (RK4), and for the initial conditions $x_{1,3,5} = 0.01$ and $x_{2,4,6} = 0.04$ the normal dynamics are given in Fig. 4. Fig. 3 shows the block diagram of the heart in its regular state.

A comparison between the ECG signal obtained digitally from system (1) (Fig. 5b [57],: time traces of ECG signal; Fig. 5c: phase portrait of ECG signal) and the ECG signal obtained from a real recording [57] (Fig. 5a) is imade. This analysis is observed in Fig. 5, on the signal produced, it is observed the presence of the five (05) main waves allowing the contraction of the heart cells, namely the P wave, the QRS complex regrouping the Q, R and S waves and finally the T wave.

4. Nonlinear computational tools/approaches

In recent years, great progress has been made in the diagnosis of arrhythmias. Indeed, some abnormalities are sometimes asymptomatic and develop without the patient decerning any signs. In this situation, the analysis of the ECG signal becomes important as it allows the detection and analysis of any heart rhythm problem.

It should be noted, however, that this is a complement to the doctor's predictions. Today, a large number of approaches are being explored to address cardiac activity-related disturbances. These studies are done to understand the causes of arrhythmias in order to improve the mechanisms related to their origin. In this section, using the tools of nonlinear analysis, a better understanding of the pathological mechanisms will be analyzed. This study is proposed with the aim of investigating the elements that are involved in the genesis of arrhythmias, cardiac cells or molecules. For this purpose, the ECG will be analyzed by plottng the bifurcation diagrams associated with their respective maximum Lyapunov exponents.

The bifurcation diagram is a representation of the abscissa $x(t_i + h)$ in the plane (η, x) [58,59] where η is a parameter of the differential system called control parameter when it is incremented. h is the integration step. To plot the bifurcation diagram, the Runge-Kutta integration method of order 4 (RK4) is used because it is stable and accurate. For $\dot{\theta}_{\eta+1} < 0$ and $\dot{\theta}_{\eta-1} > 0$, simultaneously verified, the tracing of $x(\eta)$ is performed. $\dot{\theta}_{\eta+1}$ and $\dot{\theta}_{\eta-1}$ are respectively the speed of x at a time t and its speed at the previous time.

To acquire the most information when study of a dynamic system is performed, its maximum Lyapunov exponent is generally analyzed [58,59]. It is a curve that shows a large number of dynamic behaviors that is not always known. Among these information, it is noted the chaotic behavior that is illustrated by a positive maximum Lyapunov exponent (Mahdy et al., 2020; [60]. By evaluating a maximal Lyapunov exponent, the evolution of small perturbations of the system during its evolution over time can be performed. Thus, for a positive maximal Lyapunov exponent, a stretch occurs at the separation of initially neighboring points: this is chaos. Moreover, for a negative exponent, there is a contraction or approach that characterizes a unique oscillatory or static state: this is regularity. And, finally, for a zero exponent, we have a set of quasiperiodic waveforms which in some cases is the torus.

To gain the most information when studying a dynamic system, its maximum Lyapunov exponent is usually analyzed [58,59]. This is a curve that exhibits a large number of dynamic behaviors that are not always known. Amongst this information is the chaotic behavior which is illustrated by a positive maximum Lyapunov exponent. The evaluation of a maximum Lyapunov exponent allows the evolution of small perturbations of the system to be realized during its evolution in time. Thus, for a positive maximum Lyapunov exponent, a stretch occurs at the separation of initially adjacent points: this is chaos. On the other hand, for a negative exponent, there is a contraction or approximation that is characteristic of a unique oscillatory or static state: this is regularity. And finally, for a zero exponent, there is a set of quasiperiodic waveforms which, in some cases, is the torus.

The parameters used as bifurcation parameters are: the coupling parameters k_{3-1} and k_{5-2}, and the amplitude of the external stimulus σ_1. This study is done when the heart system is not subjected to any external stimuli and also when external stimuli are considered

Considering system (1), when the dynamics of the ECG signal is taken into account, the new system is given by equation (4).

$$\begin{cases} \dot{x}_1 = x_2 \\ \dot{x}_2 = F_1(t) - \alpha_1(x_1 - v_1)(x_1 - v_2)x_2 - \dfrac{\omega_{01}^2}{e_1 d_1}x_1(x_1 + d_1)(x_1 + e_1) + k_{1-3}(x_3(t - \tau_{1-3}) - x_1) \\ \qquad + k_{1-5}(x_5(t - \tau_{1-5}) - x_1) \\ \dot{x}_3 = x_4 \\ \dot{x}_4 = F_2(t) - \alpha_2(x_3 - v_3)(x_3 - v_4)x_4 - \dfrac{\omega_{02}^2}{e_2 d_2}x_2(x_3 + d_2)(x_3 + e_2) + k_{3-1}(x_1(t - \tau_{3-1}) - x_3) \\ \qquad + k_{3-5}(x_5(t - \tau_{3-5}) - x_3) \\ \dot{x}_5 = x_6 \\ \dot{x}_6 = F_3(t) - \alpha_3(x_5 - v_5)(x_5 - v_6)x_6 - \dfrac{\omega_{03}^2}{e_3 d_3}x_5(x_5 + d_3)(x_5 + e_3) + k_{5-3}(x_3(t - \tau_{5-3}) - x_5) \\ \qquad + k_{5-1}(x_1(t - \tau_{5-1}) - x_5) \\ \dot{X} = \mu_1 x_2 + \mu_2 x_4 + \mu_3 x_6 \\ \dot{Y} = \mu_1 \dot{x}_2 + \mu_2 \dot{x}_4 + \mu_3 \dot{x}_6 \end{cases} \tag{4}$$

By perturbing system (4) by introducing small variations $e_{x_1}, e_{x_2}, e_{x_3}, e_{x_4}, e_{x_5}, e_{x_6}, e_X$ and e_Y in each of its axes, as given by equations (5) and (6)

$$
\begin{aligned}
x_1 &\rightarrow x_1 + e_{x_1} \\
x_2 &\rightarrow x_2 + e_{x_2} \\
x_3 &\rightarrow x_3 + e_{x_3}
\end{aligned}
\tag{5}
$$

$$
\begin{aligned}
x_4 &\rightarrow x_4 + e_{x_4} \\
x_5 &\rightarrow x_5 + e_{x_5} \\
x_6 &\rightarrow x_6 + e_{x_6} \\
X &\rightarrow X + e_X \\
Y &\rightarrow Y + e_Y
\end{aligned}
\tag{6}
$$

The error matrix is given in equation (7)

$$
M = \begin{bmatrix}
0 & 1 & 0 & 0 & 0 & 0 & 0 & 0 \\
a_{21} & a_{22} & 0 & 0 & 0 & 0 & 0 & 0 \\
0 & 0 & 1 & 0 & 0 & 0 & 0 & 0 \\
k_{3-1} & \tau_{3-1}k_{3-1} & a_{43} & a_{44} & 0 & 0 & 0 & 0 \\
0 & 0 & 0 & 0 & 0 & 1 & 0 & 0 \\
0 & 0 & k_{5-3} & \tau_{5-3}k_{5-3} & a_{65} & a_{66} & 0 & 0 \\
0 & \mu_1 & 0 & \mu_2 & 0 & \mu_3 & 0 & 0 \\
a_{81} & a_{82} & a_{83} & a_{84} & a_{85} & a_{86} & 0 & 0
\end{bmatrix}
\tag{7}
$$

The parameters of this matrix are given by equations (8)–(12)

$$
a_{21} = \alpha_1 x_2 \left(-2x_1 + (v_1 + v_2)x_2 \right) - \frac{\omega_{01}^2}{e_1 d_1} \left(3x_1^2 + 2(d_1 + e_1)x_1 + d_1 e_1 \right)
$$

$$
a_{22} = \alpha_1 x_1 \left(-x_1 + (v_1 + v_2)x_1 \right) - \alpha_1 v_1 v_2
$$

$$
a_{43} = \alpha_2 x_4 \left(-2x_3 + (v_3 + v_4)x_4 \right) - k_{3-1} - \frac{\omega_{02}^2}{e_2 d_2} \left(3x_3^2 + 2(d_2 + e_2)x_3 + d_2 e_2 \right)
\tag{8}
$$

$$
a_{44} = \alpha_2 x_3 \left(-x_3 + (v_3 + v_4)x_3 \right) - \alpha_2 v_3 v_4
$$

$$
a_{65} = \alpha_3 x_6 \left(-2x_5 + (v_5 + v_6)x_6 \right) - k_{5-2} - \frac{\omega_{03}^2}{e_3 d_3} \left(3x_5^2 + 2(d_3 + e_3)x_5 + d_3 e_3 \right)
$$

$$
a_{66} = \alpha_3 x_5 \left(-x_5 + (v_5 + v_6)x_5 \right) - \alpha_3 v_5 v_6
$$

$$
a_{81} = \mu_1 \left[\alpha_1 x_2 \left(-2x_1 + (v_1 + v_2)x_2 \right) - \frac{\omega_{01}^2}{e_1 d_1} \left(3x_1^2 + 2(d_1 + e_1)x_1 + d_1 e_1 \right) \right] + \mu_2 k_{3-1}
\tag{9}
$$

$$
a_{82} = \mu_1 \left[\alpha_1 x_1 \left(-x_1 + (v_1 + v_2)x_1 \right) \right] - \mu_2 \tau_{3-1} k_{3-1}
$$

$$
a_{83} = \mu_2 \left[\alpha_2 x_4 \left(-2x_3 + (v_3 + v_4)x_4 \right) - k_{3-1} - \frac{\omega_{02}^2}{e_2 d_2} \left(3x_3^2 + 2(d_2 + e_2)x_3 + d_2 e_2 \right) \right] + \mu_3 k_{5-3}
\tag{10}
$$

$$
a_{84} = \mu_2 \left[\alpha_2 x_3 \left(-x_3 + (v_3 + v_4)x_3 \right) - \alpha_2 v_3 v_4 \right] - \mu_3 \tau_{5-3} k_{5-3}
$$

$$
a_{86} = \mu_3 \left[\alpha_3 x_5 \left(-x_5 + (v_5 + v_6)x_5 \right) - \alpha_3 v_5 v_6 \right]
\tag{11}
$$

$$
a_{85} = \mu_3 \left[\alpha_3 x_6 \left(-2x_5 + (v_5 + v_6)x_6 \right) - k_{5-2} - \frac{\omega_{03}^2}{e_3 d_3} \left(3x_5^2 + 2(d_3 + e_3)x_5 + d_3 e_3 \right) \right]
\tag{12}
$$

All these analyses allow to define in equation (13) the maximum Lyapunov exponent

$$
\lambda_{Max} = \lim_{t \to \infty} \frac{1}{t} \sqrt{e_{x_1}^2 + e_{x_2}^2 + e_{x_3}^2 + e_{x_4}^2 + e_{x_5}^2 + e_{x_6}^2 + e_X^2 + e_Y^2}
\tag{13}
$$

To obtain the error matrix given by equation (7), the Taylor series expansion is used [54,61]. Starting from the equation below (14) (where τ represents the propagation delay and $\dot{x}(t)$ the temporal derivative of $x(t)$)

$$
x(t - \tau) = x(t) - \tau \dot{x}(t)
\tag{14}
$$

This allows us to simplify the lagged variables in system (4). Thus the derivation of equation (14), allows to obtain equation (15).

$$
\dot{x}(t - \tau) = \dot{x}(t) - \tau \ddot{x}(t)
\tag{15}
$$

According to the reasoning of equations (14) and (15), following the same logic for the case of system (4), the error matrix is given by equation (7)

4.1. Numerical results

The results presented below are obtained for a simulation step representing the integration step of RK4. The control parameter variation step is given by $h_a = 0.0128$. Bifurcation curves are plotted only for the ECG case

In this subsection, we will first present the results of the tests when the heart is considered in its state of no external stimulus. $(F_1(t) = F_2(t) = F_3(t) = 0)$.

Firstly, when the coupling coefficient between the AV node and the SA node k_{3-1} is taken as the bifurcation parameter, maintaining the other parameters of Table 1 except for $k_{5-3} = 20$, the bifurcation curve associated with its maximum Lyapunov exponent are given in Fig. 6. In this figure, the electrical activity reveals the presence of periodic, quasiperiodic and chaotic behaviors. A better summary for the characterization of these different behaviors observed on the bifurcation diagram of the ECG signal is given in Table 2.

To materialize these different behaviors observed on the ECG signal, some curves illustrating the dynamics (Fig. 7a, b, 7c and 7d) of the time series and the state space of the ECG are given in Fig. 7.

When the coupling parameter between the AV node and the SA node varies, the ECG shows dynamics that may indicate the presence of arrhythmias. These observations show that when the electrical impulse is initiated by the SA node, its transition from the atria to the AV node can be relevant to the heart because under certain conditions arrhythmias can occur. In this case, several types of pathology are noted, including.

- Ventricular flutter: it is represented by Fig. 7a (case of $k_{3-1} = 0.57$). It is another form of ventricular tachycardia with a very high frequency that prevents the heart from playing its pumping role and causes loss of consciousness and a sudden interruption of breathing [62].
- It is also a gateway to ventricular fibrillation. Generally poorly tolerated, it is illustrated by ripples of the QRS complexes, distinguished by equal size with an absence of an isoelectric line and visible T wave. The QRS and ST-T complexes are not separated. Heartbeats evolve between 250 and 300/min. The comparison between the experimental ECG (Fig. 8a [57]) and synthetic ECG considered (Fig. 8b) is shown in Fig. 8.
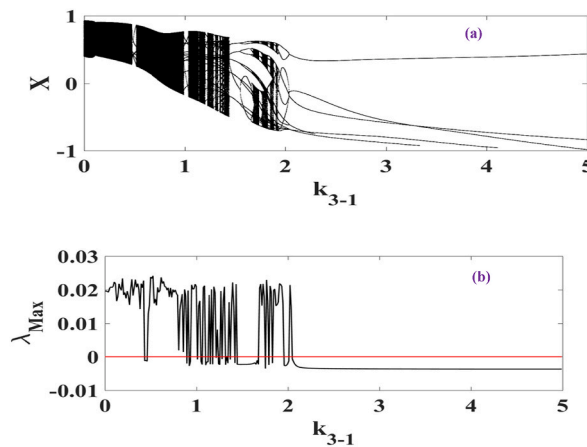

Fig. 6. (a): Bifurcation tree and maximum; (b): Lyapunov exponent obtained from system (4) with as parameter k_{3-1} for $x_{1,3,5} = 0.01$ and $x_{2,4,6} = 0.04$

Table 2
ECG dynamics for a variation of k_{3-1}

Rank of the parameter k_{3-1}	ECG behaviors
$0 < k_{3-1} \leq 0.577$	Chaotic orbit
$0.577 < k_{3-1} \leq 0.617$	Period-5T orbit
$0.617 < k_{3-1} \leq 0.894$	Chaotic orbit
$0.843 < k_{3-1} \leq 0.894$	Period-8T orbit
$0.894 < k_{3-1} \leq 1.14$	Chaos orbit
$1.14 < k_{3-1} \leq 1.21$	Period-12T orbit
$1.21 < k_{3-1} \leq 1.567$	Chaos orbit
$1.567 < k_{3-1} \leq 1.74$	Period-13T orbit
$1.74 < k_{3-1} \leq 1.894$	Orbite chaotique
$1.894 < k_{3-1} \leq 2.31$	Period-8T orbit
$2.31 < k_{3-1} \leq 2.556$	Period-5T orbit
$2.556 < k_{3-1} \leq 4.121$	Period-5T orbit
$4.121 < k_{3-1} \leq 5.0$	Period-4T orbit

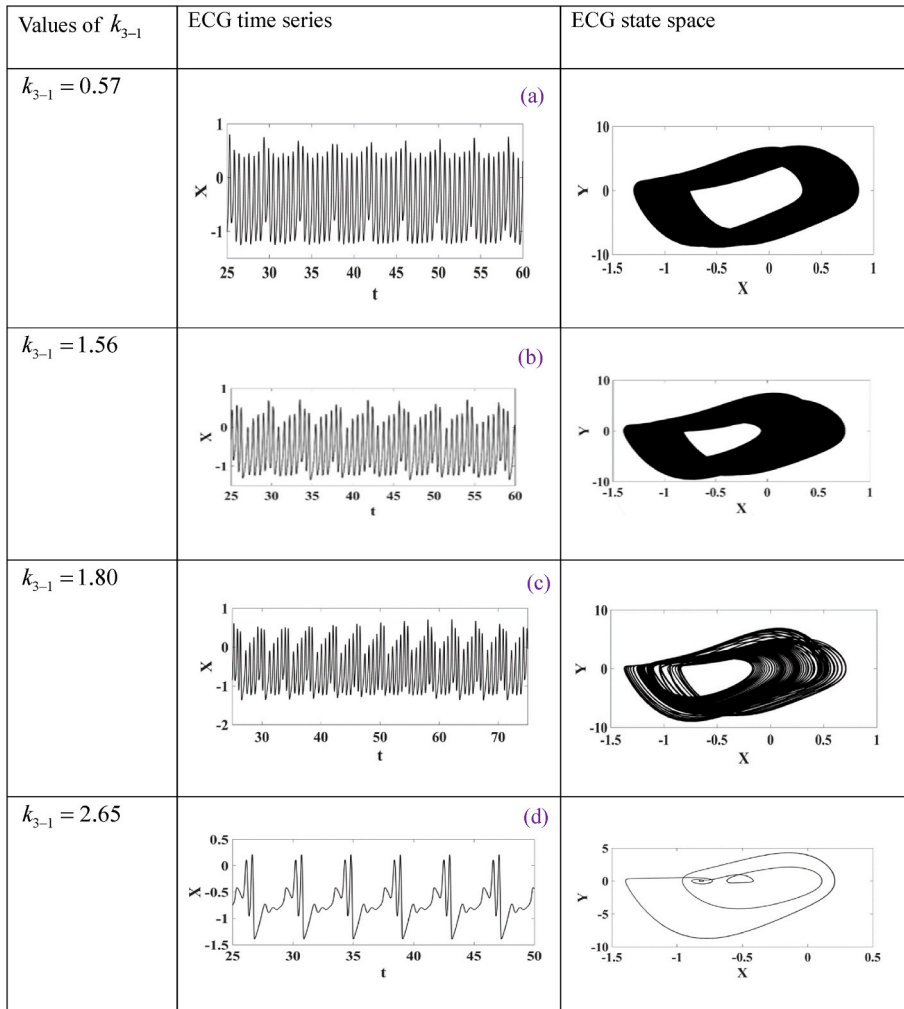| Values of k_{3-1}	ECG time series	ECG state space
$k_{3-1} = 0.57$	(a)	
$k_{3-1} = 1.56$	(b)	
$k_{3-1} = 1.80$	(c)	
$k_{3-1} = 2.65$	(d)	

Fig. 7. Dynamics describing the behavior of the heart for a variation of k_{3-1} (panel 1: Values of k_{3-1}; panel 2: ECG time series; panel 3: ECG state space).

- Ventricular fibrillation: this is illustrated in Fig. 7b and c. It is an extremely serious arrhythmia provoking a high beat of the ventricles (above 250 times per minute) mechanically preventing their contraction [63]. It can be considered as the equivalent of a cardiac arrest that can lead to sudden death in a few minutes. Faced with a marked alteration of the heart, it can follow ventricular tachycardia. Fig. 9 [63], compares the experimental ECG (Fig. 9a) with synthetic ECG considered (Fig. 9b)

The informations given in Figs. 7–9 clearly shows the transition from ventricular flutter to ventricular fibrillation.

Secondly, considering the coupling between Purkinje fibers and the AV node k_{5-3} as bifurcation parameter with $k_{3-1} = 5.0$, for the other parameters of Table 1 being kept constant, the bifurcation diagram associated with the maximum Lyapunov exponent are given in Fig. 10. In this figure, the electrical activity reveals the presence of chaotic dynamics reflecting the presence of pathologies in the heart. It is also observed periodic and quasi-periodic dynamics. Table 3 makes a synthesis of these different behaviors and some dynamics describing the time series and state space of the ECG confirming these analysis are given in Fig. 11.

Fig. 11a, b and 11c illustrate some dynamics obtained. Thus, for a change in the coupling coefficient between the Purkinje His bundle and the AV node, for values representing positive amplitudes of the maximum Lyapunov exponent, ventricular tachycardia pathology is observed (Fig. 11a). Biologically, this coupling coefficient corresponds to the electrical impulse passing from the atria to the ventricles through the AV node.

Ventricular tachycardia is an arrhythmia in which rhythm disturbances lead to very rapid contractions of the lower chambers of the heart (ventricles) (Katritsis et al., 2004). One cause is the lack of synchronization between the electrical impulses of the heart. People with some type of disease, such as heart valve disease, are usually at greatest risk of ventricular tachycardia. Chest pain, fainting, dizziness and shortness of breath are the most common signs of ventricular tachycardia. In this case, the rhythm can be slowed down by taking medication. It can also be slowed by surgery and implantation of a device. The experimental ECG signal showing the shape of a
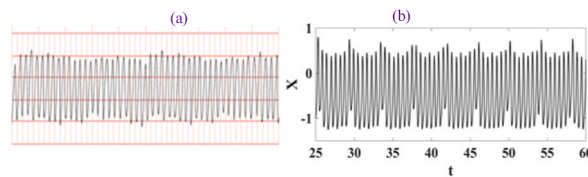
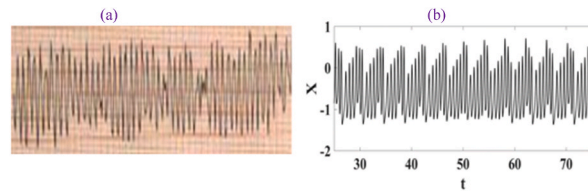**Fig. 8.** ECG signal. (a): Recorded experimental ECG signal [57]; (b): Synthetic ECG considered.

Fig. 9. ECG signal. (a): Recorded experimental ECG signal [63]; (b): Synthetic ECG considered.
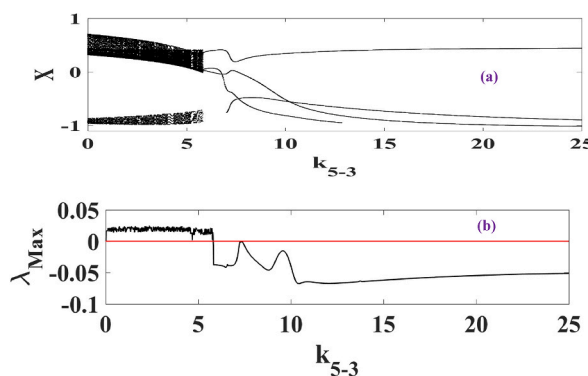

Fig. 10. (a): Bifurcation tree and maximum; (b): Lyapunov exponent obtained from system (4) with as parameter k_{5-3} for $x_{1,3,5} = 0.01$ and $x_{2,4,6} = 0.04$

Table 3
ECG dynamics for a variation of k_{5-3}

Rank of the parameter k_{5-3}	ECG behaviors
$0 < k_{5-3} \leq 5.76$	Chaotic orbit
$5.76 < k_{5-3} \leq 7.04$	Period-3T orbit
$7.04 < k_{5-3} \leq 12.84$	Period-4T orbit
$12.84 < k_{5-3} \leq 25.0$	Period-3T orbit

ventricular tachycardia is given in Fig. 12, it makes a comparison with the synthetic ECG given in Fig. 11a.

The block diagram of the core operations corresponding to the whole of its analysis is the one shown in Fig. 3.

By examining the effect of external cardiac pacemakers ($F_1(t) = F_2(t) = F_3(t) \neq 0$), the diagram of the normal functioning of the heart system is given in Fig. 13

Considering firstly amplitude β_1 as control parameter with $\omega_1 = \omega_2 = \omega_3 = 13.33$, $\beta_2 = 1.0$ and $\beta_3 = 20.0$, the results obtained are given in Fig. 14. They are obtained by maintaining the other parameters of Table 1. The information given in Fig. 14 reveals the presence of periodic, multi-periodic, and chaotic behaviors. A summary of these behaviors is given in Table 4. In order to confirm the information revealed by Table 4, some times series and state spaces of the ECG are given in Fig. 15

The observations made on the curves in Fig. 15 reveal the presence of chaotic dynamics (Fig. 15b and d) reflecting cardiac rhythm disorders. One of these arrhythmias is ventricular fibrillation. This pathology is given by the dynamics of Fig. 15d.
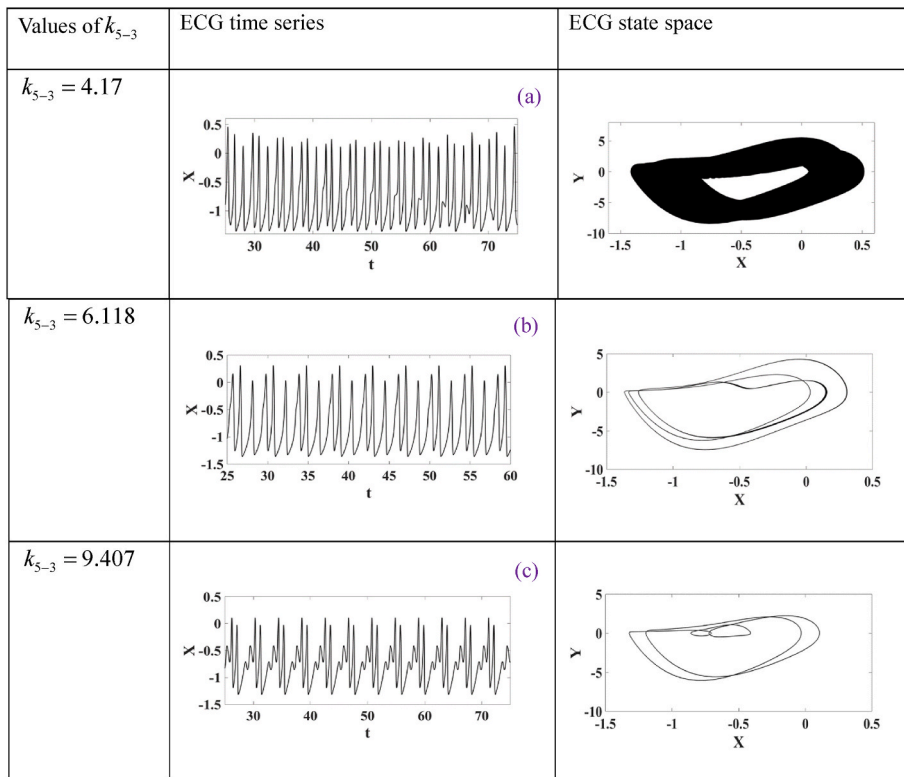
Values of k_{5-3}	ECG time series	ECG state space
$k_{5-3} = 4.17$	(a)	
$k_{5-3} = 6.118$	(b)	
$k_{5-3} = 9.407$	(c)	

Fig. 11. Dynamics describing the behavior of the heart for a variation of k_{5-3} (panel 1: Values of k_{5-3}; panel 2: ECG time series; panel 3: ECG state space).
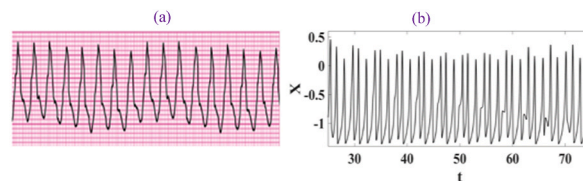

Fig. 12. ECG signal. (a): Recorded experimental ECG signal (Katritsis et al., 2004); (b): Synthetic ECG considered.
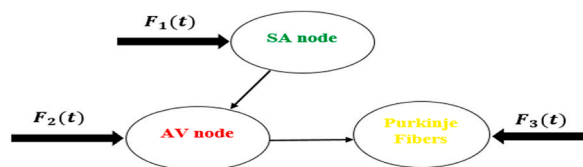

Fig. 13. Conceptual diagram of the normal functioning of heart activity under external stimuli.

Being the most frequent cardiac pathology because affecting more than 1% of the population, atrial fibrillation results in poor blood circulation because the heart rhythm is irregular and very rapid [64]. Between the atria and the ventricles, the heartbeats are not synchronized. Its particularity is that in some cases it does not present any symptoms. However, palpitations, shortness of breath, and fatigue may occur. In the case of atrial fibrillation, the speed of the electrical impulse through the two atria can be greater than 400 impulses per minute. In this situation, the ventricles respond by contracting irregularly between 80 and 180 times per minute. Thus, the blood stays longer, provoking the formation of clots in the heart chambers. The clots formed generally disperse in the circulation and a cerebral vascular accident occurs when these clots reach an artery in the brain. The ECG obtained from a real recording is given
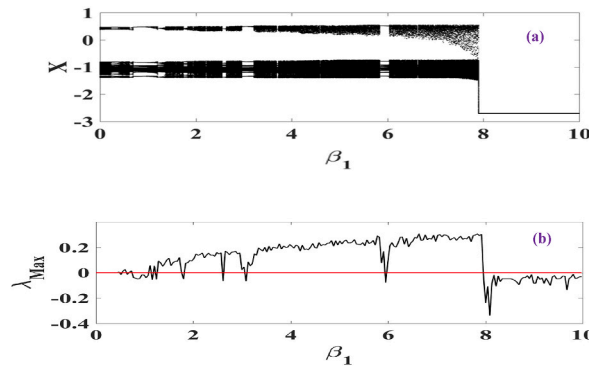
Fig. 14. (a): Bifurcation tree and maximum; (b): Lyapunov exponent obtained from system (4) with as parameter β_1 for $x_{1,3,5} = 0.01$ and $x_{2,4,6} = 0.04$

Table 4
ECG dynamics for a variation of β_1

Rank of parameter β_1	ECG behaviors
$0 < \beta_1 \leq 0.9844$	Period-14T orbit
$0.9844 < \beta_1 \leq 1.754$	Chaotic orbit
$1.754 < \beta_1 \leq 1.8$	Period-12T orbit
$1.8 < \beta_1 \leq 2.568$	Chaotic orbit
$2.568 < \beta_1 \leq 2.68$	Period-17T orbit
$2.68 < \beta_1 \leq 3.0388$	Orbite chaotique
$3.0388 < \beta_1 \leq 3.0826$	Period-14T orbit
$3.0826 < \beta_1 \leq 5.9064$	Chaotic orbit
$5.9064 < \beta_1 \leq 5.9492$	Period-13T orbit
$5.9492 < \beta_1 \leq 7.918$	Chaotic orbit
$7.918 < \beta_1 \leq 10.0$	Period-1T orbit

in Fig. 16a and a [64], comparison with the synthetic signal (Fig. 16b) is shown in Fig. 16.

Secondly, still considering the amplitude β_1 as bifurcation parameter with $\omega_1 = \omega_2 = \omega_3 = 7.33$, $\beta_2 = 1.0$ and $\beta_3 = 20.0$, always using the other parameters of Table 1 except for $\alpha_1 = 6.0$, the information brought out by the bifurcation curve and the maximum Lyapunov exponent given by Fig. 17 reveal the presence of periodic, multi-periodic and chaotic dynamics. To better interpret these different behaviors, a synthesis is made by Table 5. Fig. 18 gives some curves of the ECG through its time series and state spaces in order to confirm the analyses of Table 5.

In Fig. 18 only one curve describing chaotic behavior has been presented (Fig. 18b) because, being identical to all other chaotic curves, it was preferable to present only one. However, the information revealed by this figure is the presence of ventricular fibrillation. Thus, when the heart undergoes disturbances caused by external stimuli reflecting the action of pacemakers, the heart rhythm is in a situation of ventricular fibrillation. In contrast to the case observed in Fig. 9, this form of ventricular fibrillation is more complex and is characterised by an irregularity of the ECG with a very rapid QRS complex. The experimental signal for this form of ventricular fibrillation is given in Fig. 19a [63],. A correspondence is made with synthetic ECG considered (Fig. 19b).

Thirdly, still considering the action of external stimuli on the electrical conduction system, when the coupling coefficient k_{3-1} allowing communication between the AV node and the SA node is taken as the control parameter, the bifurcation diagram and the maximum Lyapunov exponent are given in Fig. 20. The other parameters in Table 1 are maintained except $\alpha_1 = 6.0$ and the parameter values of the external stimuli are: $\omega_1 = \omega_2 = \omega_3 = 7.33$, $\sigma_1 = 8.0$, $\sigma_2 = 1.0$ and $\sigma_3 = 20.0$. This figure shows the presence of chaotic and periodic dynamics. Table 6 gives more explanations. Some ECG curves from these time series and state space confirm the information given in Table 6. These curves show the chaotic dynamics that can explain the presence of arrhythmias and are given in Fig. 22 [63],. Among these arrhythmias it is observed the presence for certain values of k_{3-1} the pathology of ventricular flutter and for other values the presence of ventricular fibrillation. This form of ventricular fibrillation is different from the first two forms observed in Figs. 9 and 19.

Fig. 21a, b and 21c illustrate some dynamics obtained. A third form of ventricular fibrillation is observed. This third form of ventricular fibrillation pathology is given in Fig. 21c. A comparison of its ECG obtained from a real recording and the ECG of Fig. 21c is given in Fig. 22.
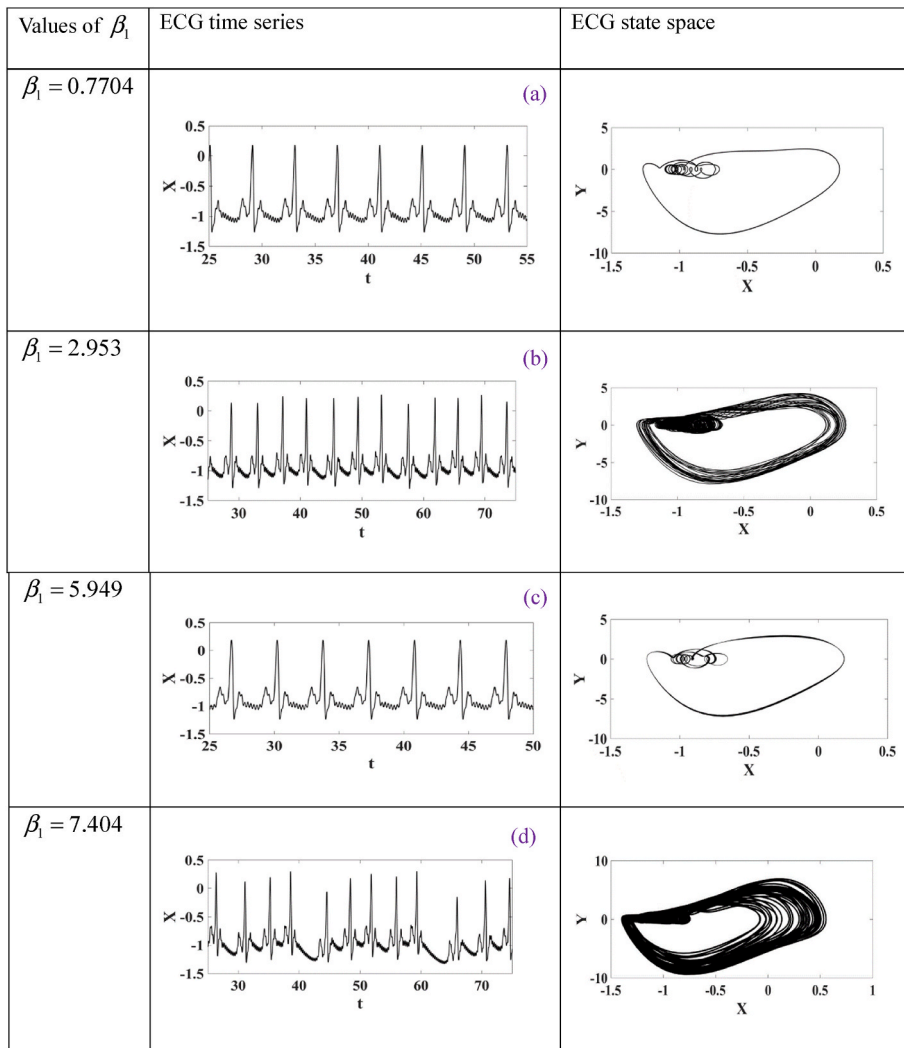
Values of β_1	ECG time series	ECG state space
$\beta_1 = 0.7704$	(a)	
$\beta_1 = 2.953$	(b)	
$\beta_1 = 5.949$	(c)	
$\beta_1 = 7.404$	(d)	

Fig. 15. Dynamics describing the behavior of the heart for a variation of β_1 (panel 1: Values of β_1; panel 2: ECG time series; panel 3: ECG state space).
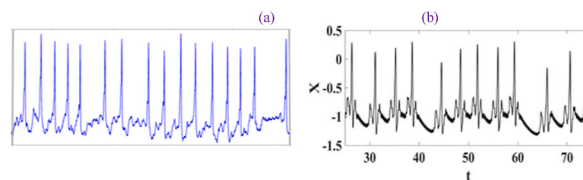

Fig. 16. ECG signal. (a): Recorded experimental ECG signal [64]; (b): Synthetic ECG considered.

5. Microcontroller real implementation

Being able to perform fast simulations, the microcontroller allows a program to be executed in real time at a chosen speed or step by step with the help of software [65]. It governs specific operations and is one of the most compact integrated circuits. Unlike circuits with analog components that have difficulties with noise, scaling and environmental disturbances, this compactness makes them very reliable and stable. Microcontrollers have a wide range of applications such as robotics, biology, artificial intelligence, telecommunications, etc. [65-67]. As pacemakers are electronic chips composed of batteries, which require a certain period of time to function, they need to be replaced and in some cases recharged. Followed by adapted controllers and attached to sensors, cardiac activity is monitored. References [46,68] have shown that the microcontroller-based differential equation conversion mechanism can be used to
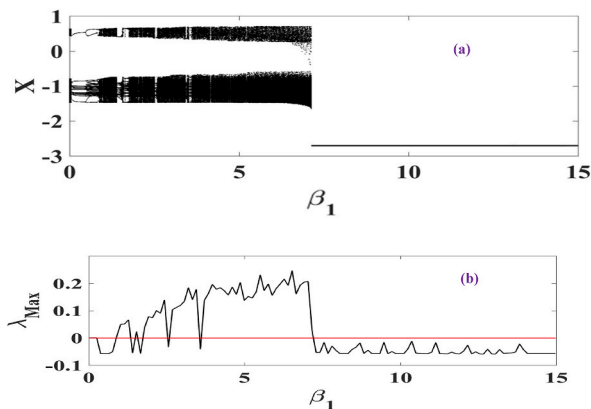
Fig. 17. (a): Bifurcation tree and maximum; (b): Lyapunov exponent obtained from system (4) with as parameter β_1 for $x_{1,3,5} = 0.01$ and $x_{2,4,6} = 0.04$

Table 5
ECG dynamics for a variation of β_1

Rank of parameter β_1	ECG behaviors
$0 < \beta_1 \leq 0.896$	Period-9T orbit
$0.896 < \beta_1 \leq 1.33$	Chaotic orbit
$1.33 < \beta_1 \leq 1.664$	Period-10T orbit
$1.664 < \beta_1 \leq 2.432$	Chaotic orbit
$2.432 < \beta_1 \leq 2.56$	Period-7T orbit
$2.56 < \beta_1 \leq 3.456$	Chaotic orbit
$3.456 < \beta_1 \leq 3.584$	Period-11T orbit
$3.584 < \beta_1 \leq 7.568$	Chaotic orbit
$7.568 < \beta_1 \leq 15.0$	Period-1T orbit

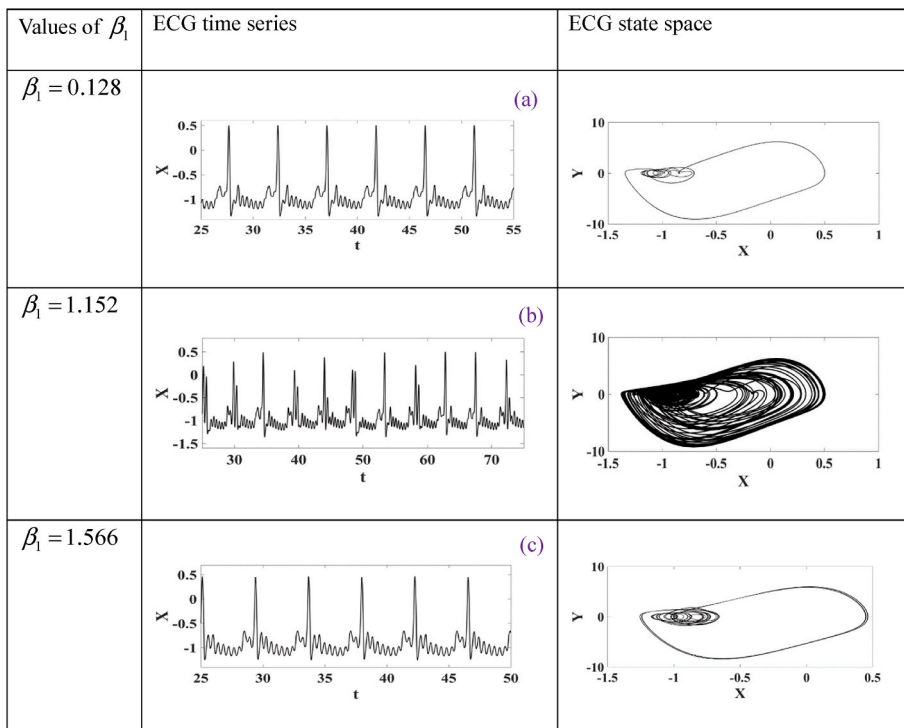| Values of β_1	ECG time series	ECG state space
$\beta_1 = 0.128$	(a)	
$\beta_1 = 1.152$	(b)	
$\beta_1 = 1.566$	(c)	

Fig. 18. Dynamics describing the behavior of the heart for a variation of β_1 (panel 1: Values of β_1; panel 2: ECG time series; panel 3: ECG state space).
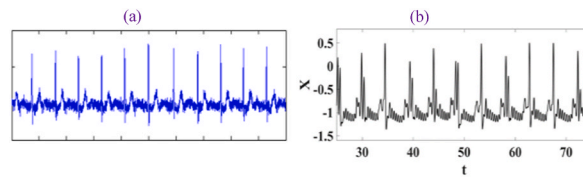
Fig. 19. ECG signal. (a): Recorded experimental ECG signal [63]; (b) Synthetic ECG considered.
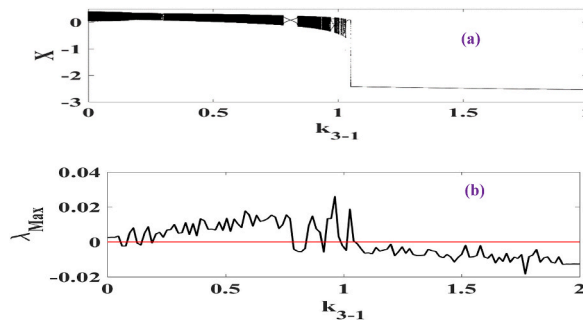

Fig. 20. (a): Bifurcation tree and maximum; (b): Lyapunov exponent obtained from system (4) with as parameter k_{3-1} for $x_{1,3,5} = 0.01$ and $x_{2,4,6} = 0.04$

Table 6
ECG dynamics for a variation of k_{3-1}

Parameter Rank k_{3-1}	ECG behaviors
$0 < k_{3-1} \leq 0.7741$	Chaotic orbit
$0.7741 < k_{3-1} \leq 0.837$	Period-2T orbit
$0.837 < k_{3-1} \leq 0.999$	Chaotic orbit
$0.999 < k_{3-1} \leq 1.0112$	Period-4T orbit
$1.0112 < k_{3-1} \leq 1.0427$	Quasiperiodic orbit
$1.0427 < k_{3-1} \leq 2.0$	Period-1T orbit

reproduce the operation of artificial pacemakers. The principle of this simulation is based on algorithms. The codes are implemented by discretization using the Runge-Kutta method or the Euler method as in the case of numerical simulation using an adequate programming language.

Considering the nodes of the heart as pacemakers, the principle of microcontroller simulation is used in this section to reproduce the functioning of the heart. To do so, four microcontrollers are used and each of the microcontrollers is used to mimic the behavior of a heart node and that of the ECG signal respectively through the algorithm contained in it. Using the principle of the normal functioning of the heart as described by the block diagrams in Figs. 3 and 13, the practical devices used are given in Figs. 23 and 24. Fig. 23 is the configuration corresponding to system (1). Fig. 23a shows the wiring mounted on Proteus and the real experimental wiring is given by Fig. 23b.

The configuration for generating the ECG signal is given in Fig. 24. The setup wired on Proteus is shown in Fig. 24a and b shows the experimental setup.

In Fig. 23 (Fig. 23a and b), each heart node is represented by an Arduino board, and each R-2R resistor network given by (a) allows the digital to analog conversion. At the output of the first Arduino board corresponding to the SA node, the signal is introduced at the input of the second Arduino board representing the AV node. The signal produced by this latter is also introduced at the input of the third Arduino board corresponding to the HP node. The signal introduced at the input of each Arduino board is converted into a digital signal thanks to the code line "analogRead (A0)" which means analog signal read at the input A0 of the board and the code line "map (a0, a01, a02, a03, a04)" which means convert the analog signal read at the input A0 into a digital signal. The argument a0 represents the input value; a01 is the extremely low input value; a02 is the extremely high input value; a03 is the extremely low output value and a04 is the extremely high output value. These different arguments are chosen randomly in order to obtain the desired dynamics.

The same reasoning is observed in Fig. 24 (Fig. 24a and b). In this figure, the Arduino board that produces the ECG signal receives at
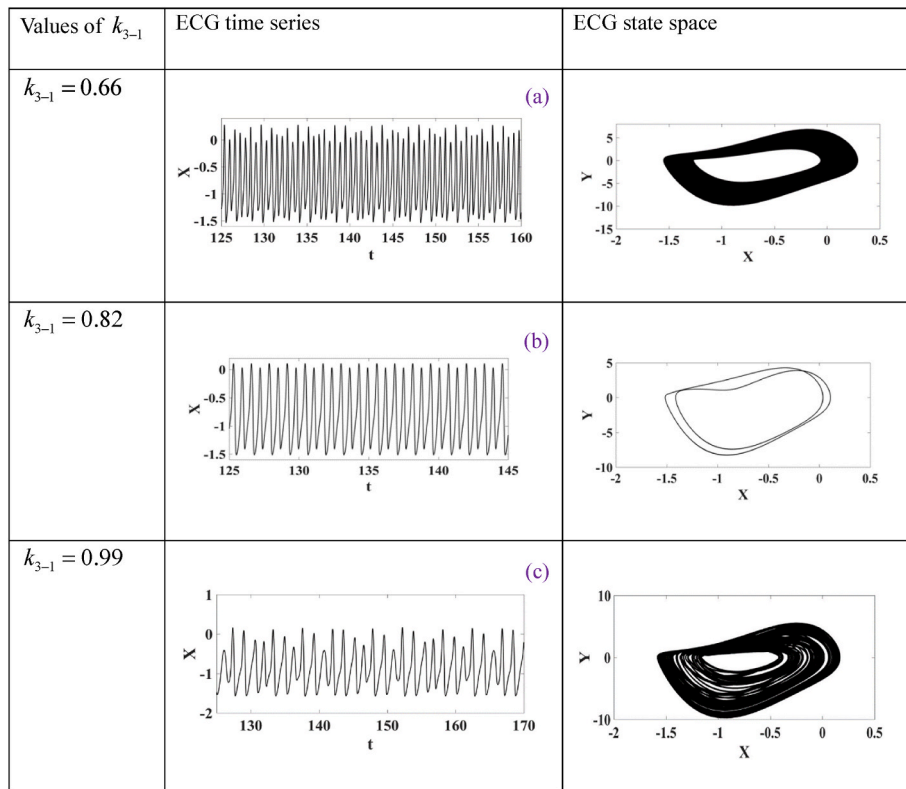
Values of k_{3-1}	ECG time series	ECG state space
$k_{3-1} = 0.66$	(a)	
$k_{3-1} = 0.82$	(b)	
$k_{3-1} = 0.99$	(c)	

Fig. 21. Dynamics describing the behavior of the heart for a variation of k_{3-1} (panel 1: Values of k_{3-1}; panel 2: ECG time series; panel 3: ECG state space).
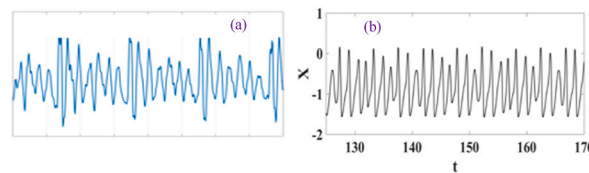

Fig. 22. ECG signal. (a): Recorded experimental ECG signal [63]; (b): Synthetic ECG considered.

its inputs the signals produced by each of the nodes. Input A0 receives the signal produced by the SA node, input A1 receives the signal produced by the AV node and input A2 receives the signal produced by the Purkinje His bundles. Thanks to the explanations allowing the digital-analog and digital-analog conversions given above for the case of Fig. 24, the ECG signal is obtained as seen on the oscilloscope. Note that the different figures (a) represent the configurations mounted on Proteus and the figures (b) those wired experimentally.

First, the results obtained in the case of a normal ECG are given. Then, the results obtained using the nonlinear analysis tools are presented initially when no external stimulus is considered and then when external stimuli are considered. The source code allowing to produce these different signals is given in Table 7.

For the case of the normal ECG, the results are given in Fig. 25.

Considering the study by nonlinear analysis for the case without external stimuli, the curves interpreting the abnormal and normal heart rhythms obtained by microcontrollers are given respectively in Fig. 26 for k_{3-1} as control parameter, in Fig. 27 for k_{5-3} as control parameter. Some curves are presented here to show the possibility of using a microcontroller network to capture the electrical activity of the heart

On the other hand, when the effects of external stimuli are taken into account, the results obtained using a microcontroller,
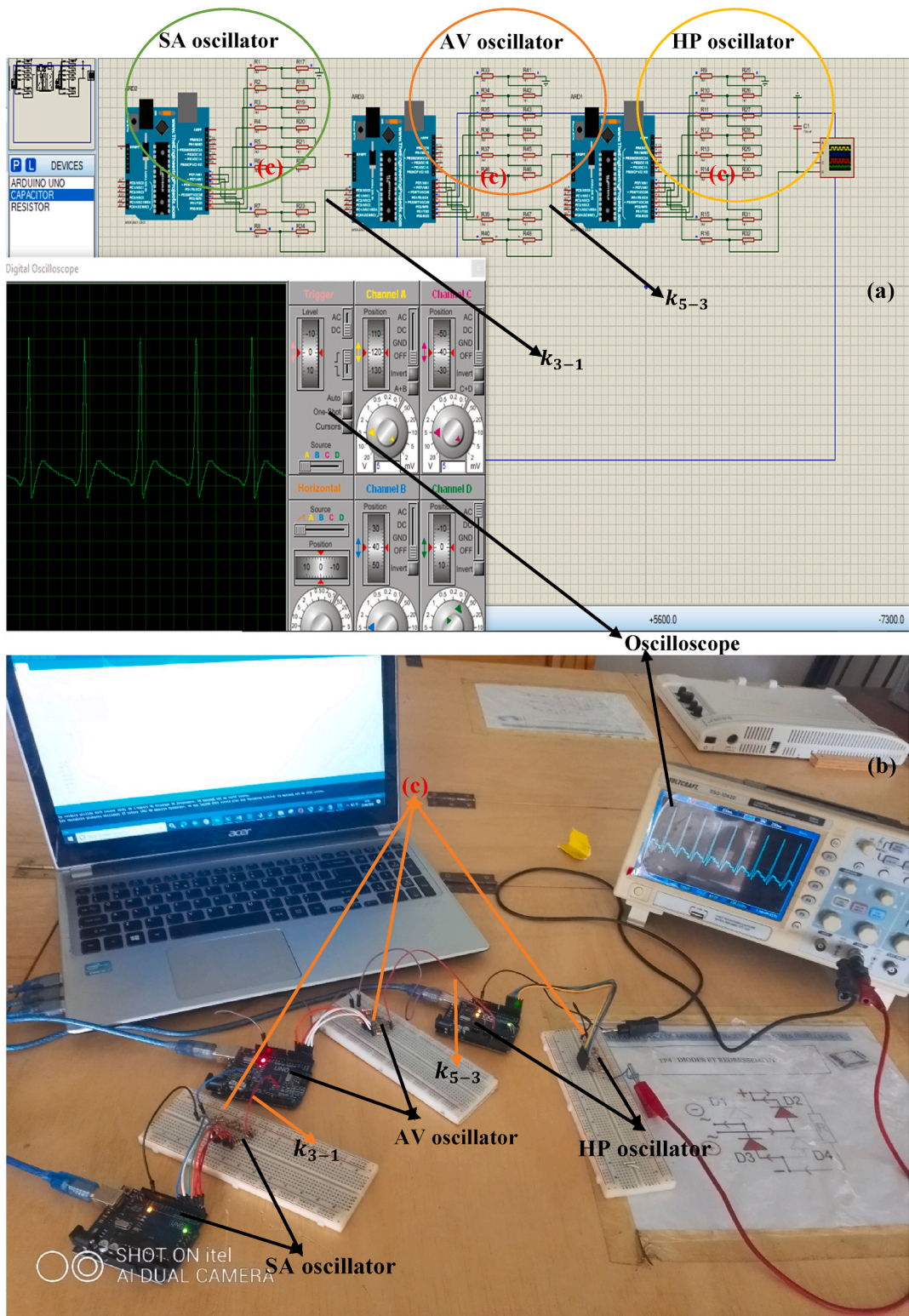
Fig. 23. Device describing the heart system given by system (1). (a) Assembly on Proteus; (b) experimental implementation.
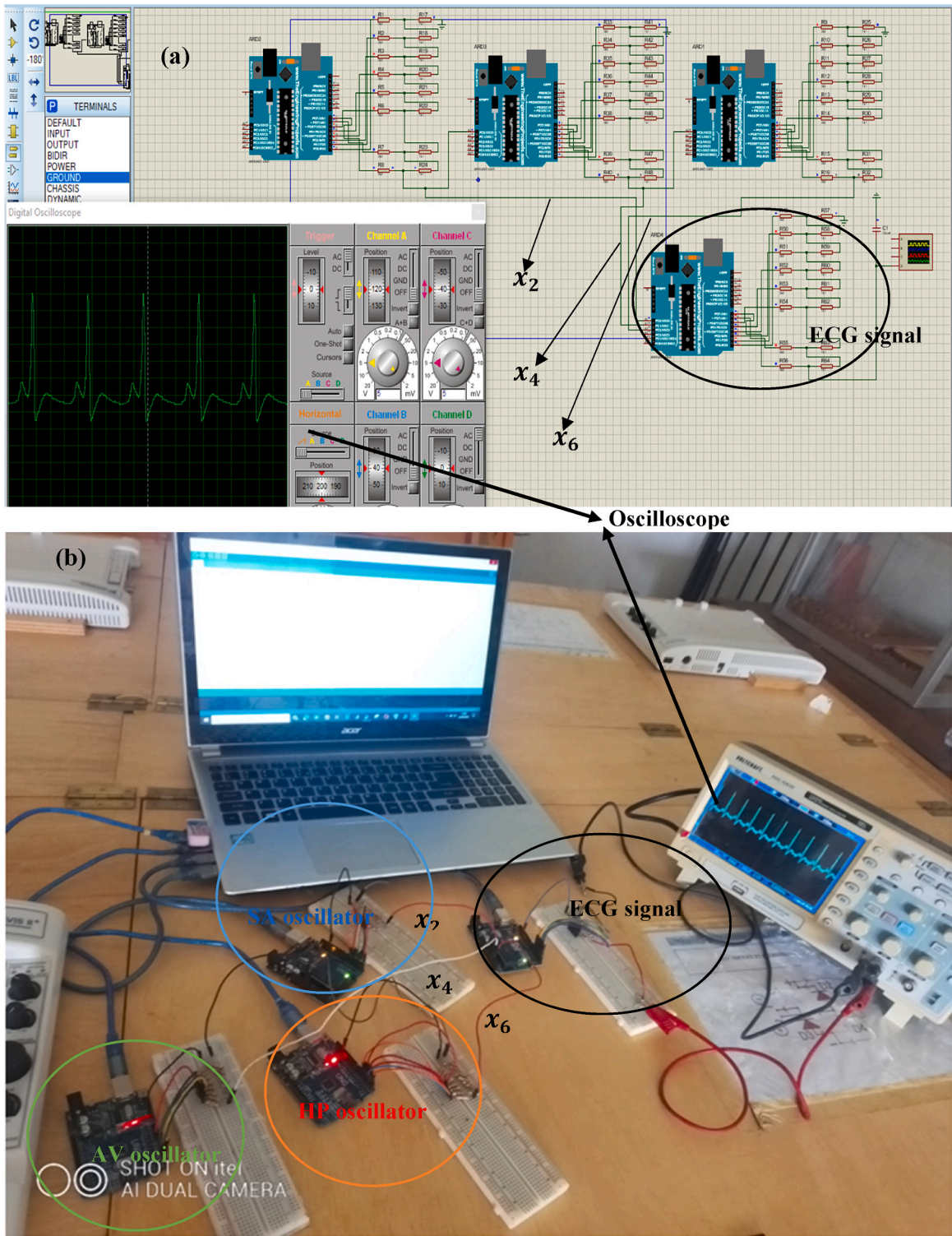
Fig. 24. Device used for the production of the ECG signal described by system (5). (a) Assembly on Proteus; (b) experimental implementation.

Table 7

Source code for the microcontroller implementation.

Produce code

```
//constants float aAV=(float)3.,aSA=(float)3.0,aHP=(float)5.;
float wAV1=(float)0.2,wSA1=(float)0.2,wHP1=(float)1.1;
float wAV2=(float)-0.1,wSA2=(float)-1.9,wHP2=(float)-1.;
float dAV=(float)3.,dSA=(float)3.,dHP=(float)3.;
float eAV=(float)3.,eSA=(float)4.9,eHP=(float)7.;
float kAVSA=(float)5.0,kHPAV=(float)20.0,h=(float)0.045;
float alpha1=(float)0.1,alpha3=(float)0.05,alpha5=(float)0.4;
float tau1=(float)0.8,tau2=(float)0.1;
//initial conditions float x1=(float)0.01,x3=(float)0.01;
float x5=(float)0.01,x2=(float)0.04;
float x4=(float)0.04,x6=(float)0.04;
float V0=(float)0.01,t1=(float)0.0;
//vriables float L1,L2,L3,L4,F1,F2,F3,F4,G1,G2,G3;
float G4,Q1,Q2,Q3,Q4,M1,M2,M3,M4;
float P1,P2,P3,P4,N1,N2,N3,N4;
float x01,x02,t,x03,x04,x05,x06;
float V01,t2;
void setup (){
pinMode (0, OUTPUT), pinMode (1, OUTPUT), pinMode (2, OUTPUT), pinMode (3, OUTPUT);
pinMode (4, OUTPUT), pinMode (5, OUTPUT), pinMode (6, OUTPUT), pinMode (7, OUTPUT);
pinMode (A0, INPUT); }
void loop (){
L1 = x2;
M1 = -aSA*x2*(x1-wSA1)*(x1-wSA2)-x1*(x1+dSA)*(x1+eSA);
N1 = x4;
P1 = -aAV*x4*(x3-wAV1)*(x3-wAV2)-x3*(x3+dAV)*(x3+eAV)-kAVSA*(x3-x1+(tau1)*x2);
Q1 = x6;
F1 = -aHP*x6*(x5-wHP1)*(x5-wHP2)-x5*(x5+dHP)*(x5+eHP)-kHPAV*(x5-x3+(tau2)*x4);
G1 = alpha1*x2+alpha3*x4+alpha5*x6; x01 = x1+(h/2)*L1, x02 = x2+(h/2)*M1, x03 = x3+(h/2)*N1, x04 = x4+(h/2)*P1;
x05 = x5+(h/2)*Q1, x06 = x6+(h/2)*F1, V01 = V0+(h/2)*G1, t = t1+(h/2);
L2 = x02;
M2 = -aSA*x02*(x01-wSA1)*(x01-wSA2)-x01*(x01 + dSA)*(x01 + eSA);
N2 = x04;
P2 = -aAV*x04*(x03-wAV1)*(x03-wAV2)-x03*(x03 + dAV)*(x03 + eAV)-kAVSA*(x03-x01+(tau1)*x02);
Q2 = x06;
F2 = -aHP*x06*(x05-wHP1)*(x05-wHP2)-x05*(x05 + dHP)*(x05 + eHP)-kHPAV*(x05-x03+(tau2)*x04);
G2 = alpha1*x02+alpha3*x04+alpha5*x06; x01 = x1+(h/2)*L2, x02 = x2+(h/2)*M2, x03 = x3+(h/2)*N2, x04 = x4+(h/2)*P2;
x05 = x5+(h/2)*Q2, x06 = x6+(h/2)*F2, V01 = V0+(h/2)*G2, t = t1+(h/2);
L3 = x02;
M3 = -aSA*x02*(x01-wSA1)*(x01-wSA2)-x01*(x01 + dSA)*(x01 + eSA);
N3 = x04;
P3 = -aAV*x04*(x03-wAV1)*(x03-wAV2)-x03*(x03 + dAV)*(x03 + eAV)-kAVSA*(x03-x01+(tau1)*x02);
Q3 = x06;
F3 = -aHP*x06*(x05-wHP1)*(x05-wHP2)-x05*(x05 + dHP)*(x05 + eHP)-kHPAV*(x05-x03+(tau2)*x04);
G3 = alpha1*x02+alpha3*x04+alpha5*x06; x01 = x1+(h)*L3, x02 = x2+(h)*M3, x03 = x3+(h)*N3, x04 = x4+(h)*P3;
x05 = x5+(h)*Q3, x06 = x6+(h)*F3, V01 = V0+(h)*G3, t = t1+(h);
L4 = x02;
M4 = -aSA*x02*(x01-wSA1)*(x01-wSA2)-x01*(x01 + dSA)*(x01 + eSA);
N4 = x04;
P4 = -aAV*x04*(x03-wAV1)*(x03-wAV2)-x03*(x03 + dAV)*(x03 + eAV)-kAVSA*(x03-x01+(tau1)*x02);
Q4 = x06;
F4 = -aHP*x06*(x05-wHP1)*(x05-wHP2)-x05*(x05 + dHP)*(x05 + eHP)-kHPAV*(x05-x03+(tau2)*x04);
G4 = alpha1*x02+alpha3*x04+alpha5*x06; x1 = x1+(h/6)*(L1+2.*L2+2.*L3+L4), x2 = x2+(h/6)*(M1+2.*M2+2.*M3+M4);
x3 = x3+(h/6)*(N1+2.*N2+2.*N3+N4), x4 = x4+(h/6)*(P1+2.*P2+2.*P3+P4);
x5 = x5+(h/6)*(Q1+2.*Q2+2.*Q3+Q4), x6 = x6+(h/6)*(F1+2.*F2+2.*F3+F4);
V0=V0+(h/6)*(G1+2.*G2+2.*G3+G4), t = t1+h;
PORTD=(V0-20)*11.5; x1 = x1; x2 = x2; x3 = x3; x4 = x4; x5 = x5; x6 = x6; V0=V0; t1 = t; }
```

describing the abnormal and normal heart rhythms are presented respectively in Fig. 28 for β_1 as control parameter with $\alpha_1 = 3.0$, in Fig. 29 for β_1 as control parameter with $\alpha_1 = 6.0$ and in Fig. 30 for k_{3-1} as control parameter. Some of the curves are represented here in the figure below

The results observed in Figs. 25–30 show a good qualitative agreement between the numerical simulation and the real micro-controller implementation. As in the case of conventional wiring to produce the ECG signal using an oscillator network with electronic components mounted on a breadboard [54], since the heart nodes are considered as electronic chips and references [47] have shown the ability of microcontrollers to mimic the behavior of pacemakers, using a network of four microcontrollers each representing a heart node and the ECG, the results obtained show the ability to use microcontroller technology to capture heart rhythms.

The results presented in this work show the ability of the model to capture the cardiac activity by the different synthetic ECG signals
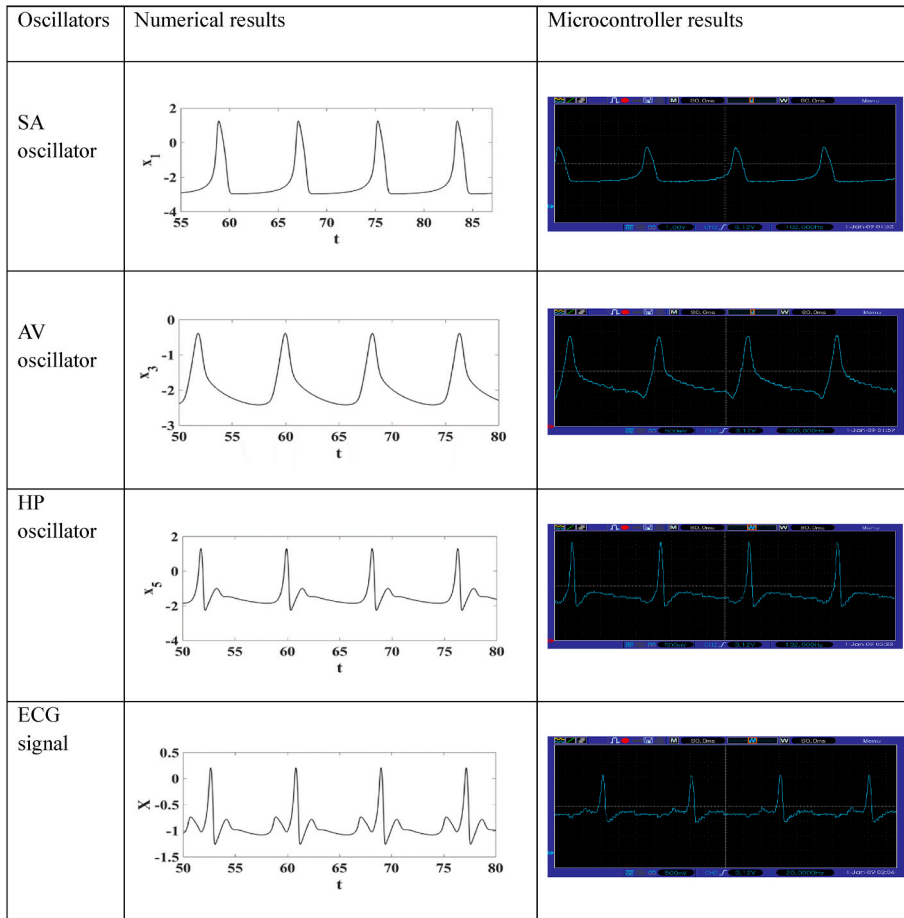
Oscillators	Numerical results	Microcontroller results
SA oscillator		
AV oscillator		
HP oscillator		
ECG signal		

Fig. 25. Dynamics of the different cardiac nodes and synthetic ECG signal obtained for $x_{1,3,5} = 0.01$ and $x_{2,4,6} = 0.04$ (panel 1: Oscillators; panel 2: Numerical results; column 3: Microcontroller results).

obtained and the different pathologies that emerged. However, the study was only interested in the shape of the wave. Thus, some aspects such as wave amplitude, duration, and interval time could also be studied [2]. The evaluation of the energy by the variation of the different coupling parameters could also bring out interesting behaviors. All of these aspects could help in a more important characterization of the physiology.

6. Conclusion

In this work, the dynamics of the heart system were studied using nonlinear analysis tools using ECG signals. For this purpose, the electrical system of the heart was considered as a network of three nonlinear oscillators representing respectively the SA node, the AV node, and the His of Purkinje bundles, and the combination of the signals produced by its different nodes allowed to generate the synthetic ECG. First, analysis by plotting the bifurcation curves associated with their respective maximal Lyapunov exponents is performed. By considering the coupling parameters representing the communication aspects between the different cardiac nodes, the amplitude of the external stimuli, and the AV node variable as a control parameter, the precise values for which the cardiac activity can be periodic, quasiperiodic, or chaotic were obtained. Evaluation of the electrocardiogram (ECG) signal presents normal and pathological rhythms. Three forms of ventricular fibrillation, two forms of ventricular flutter, ventricular tachycardia, and atrial fibrillation are presented. Second, considering the nodes of the heart as pacemakers and since they are artificially modelled as microchips, microcontroller simulation technology was used to model the cardiac system as a network of four ATmega 328P microcontrollers representing the SA node, AV node, Purkinje His bundles, and synthetic ECG respectively. The results obtained indicate a very good fit with those obtained numerically. It is observed that microcontroller simulation technology can be used to model the cardiac conduction system. The results obtained indicate that the heart rhythm activity is captured.
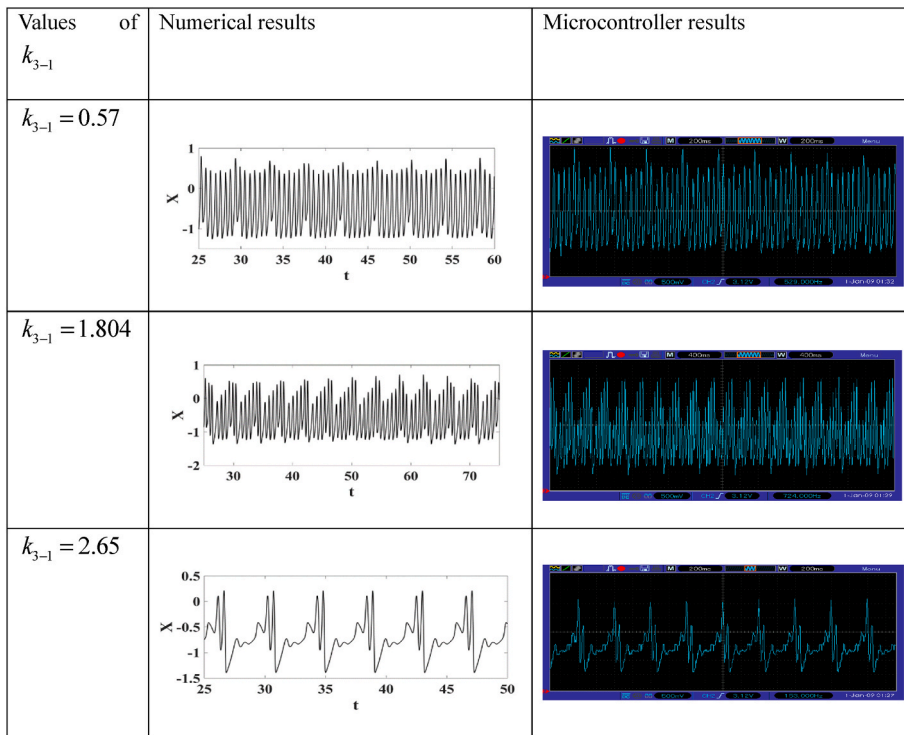
Values of k_{3-1}	Numerical results	Microcontroller results
$k_{3-1} = 0.57$		
$k_{3-1} = 1.804$		
$k_{3-1} = 2.65$		

Fig. 26. Dynamics of the different cardiac nodes and synthetic ECG signal obtained for a variation of k_{3-1} with $x_{1,3,5} = 0.01$ and $x_{2,4,6} = 0.04$ (panel 1: Oscillators; panel 2: Numerical results; column 3: Microcontroller results).
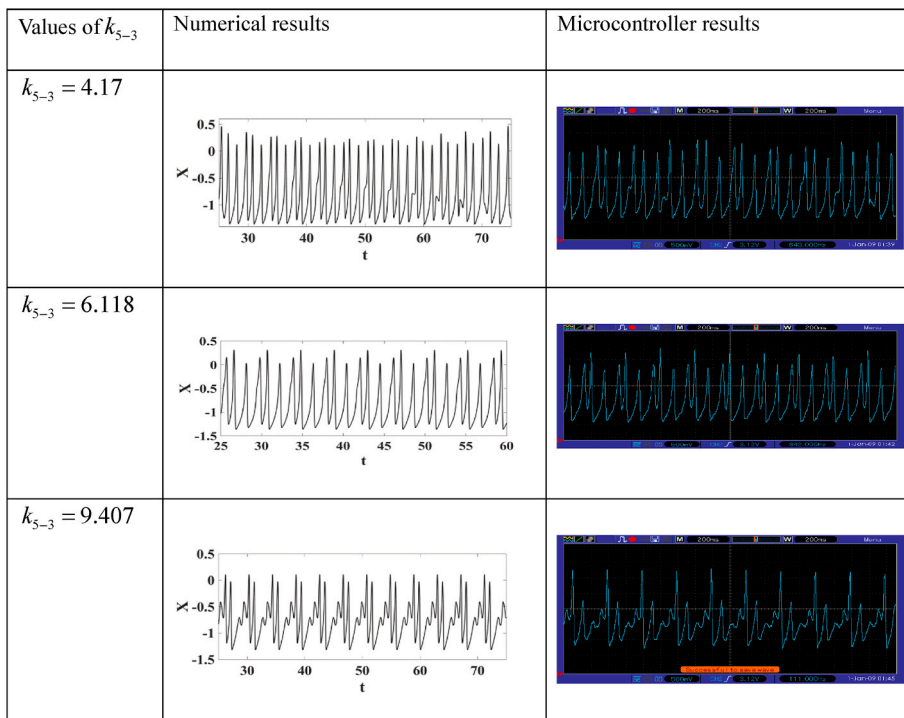
Values of k_{5-3}	Numerical results	Microcontroller results
$k_{5-3} = 4.17$		
$k_{5-3} = 6.118$		
$k_{5-3} = 9.407$		

Fig. 27. Dynamics of the different cardiac nodes and synthetic ECG signal obtained for a variation of k_{5-3} with $x_{1,3,5} = 0.01$ and $x_{2,4,6} = 0.04$ (panel 1: Oscillators; panel 2: Numerical results; column 3: Microcontroller results).
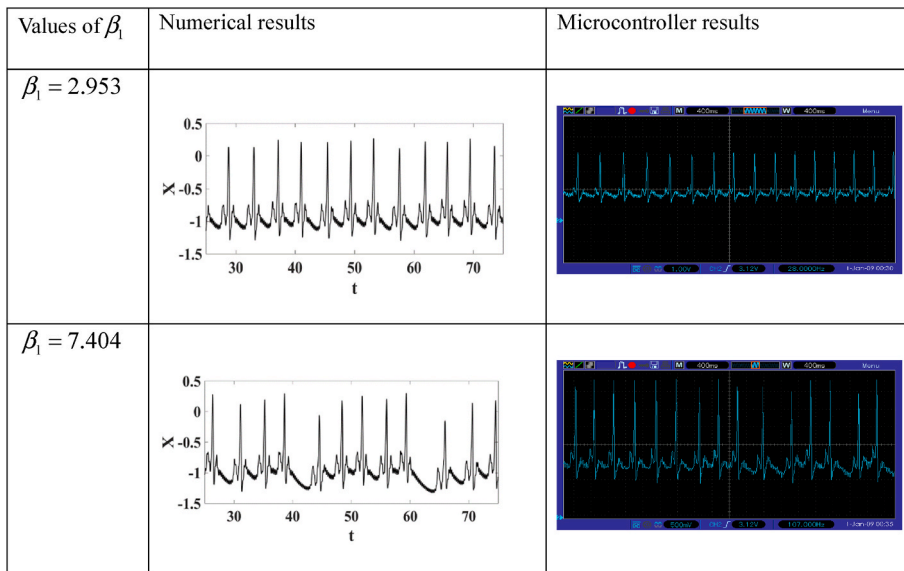
Values of β_1	Numerical results	Microcontroller results
$\beta_1 = 2.953$		
$\beta_1 = 7.404$		

Fig. 28. Dynamics of the different cardiac nodes and synthetic ECG signal obtained for a variation of β_1 with $\alpha_1 = 3.0$, $x_{1,3,5} = 0.01$ and $x_{2,4,6} = 0.04$ (panel 1: Oscillators; panel 2: Numerical results; column 3: Microcontroller results).
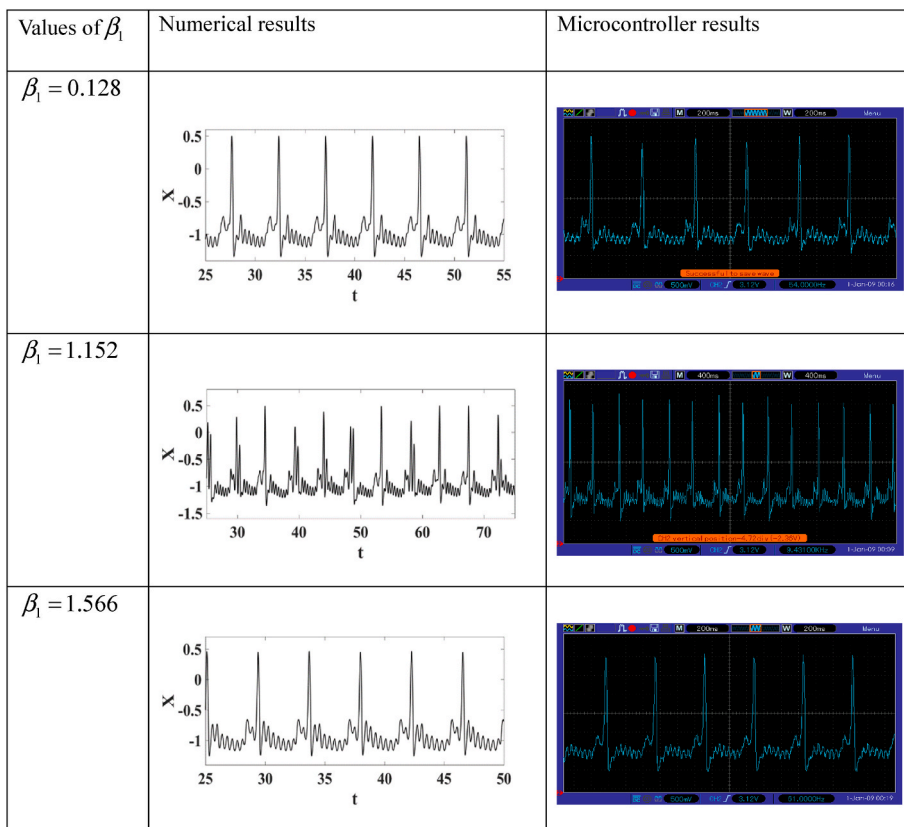
Values of β_1	Numerical results	Microcontroller results
$\beta_1 = 0.128$		
$\beta_1 = 1.152$		
$\beta_1 = 1.566$		

Fig. 29. Dynamics of the different cardiac nodes and synthetic ECG signal obtained for a variation of β_1 with $\alpha_1 = 6.0$, $x_{1,3,5} = 0.01$ and $x_{2,4,6} = 0.04$ (panel 1: Oscillators; panel 2: Numerical results; column 3: Microcontroller results).
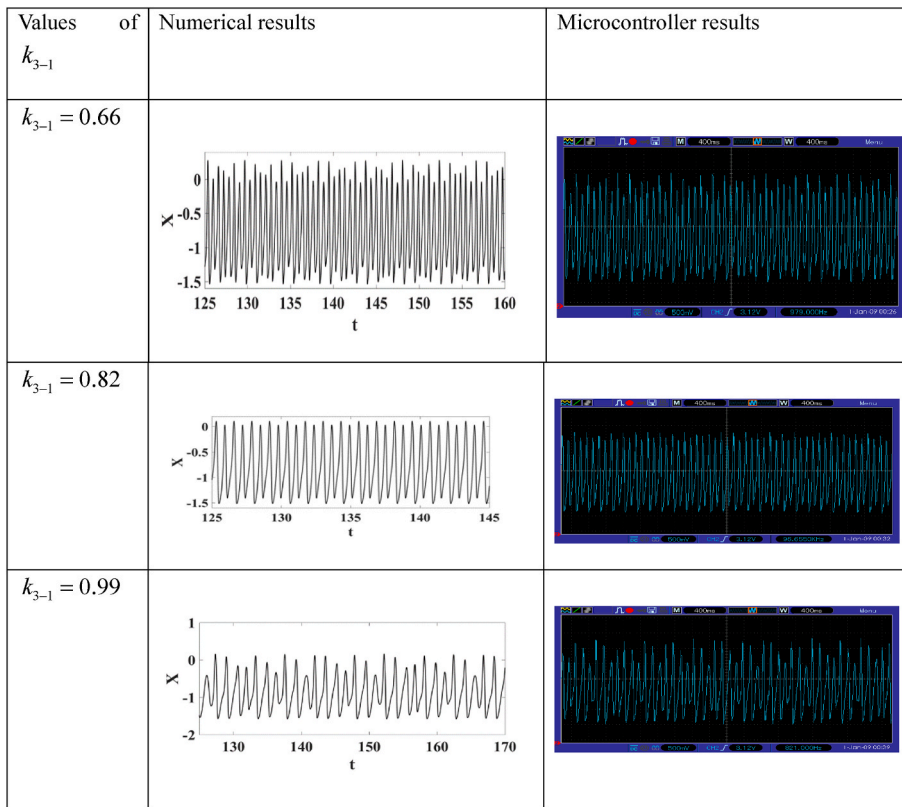
Values of k_{3-1}	Numerical results	Microcontroller results
$k_{3-1} = 0.66$		
$k_{3-1} = 0.82$		
$k_{3-1} = 0.99$		

Fig. 30. D Dynamics of the different cardiac nodes and synthetic ECG signal obtained for a variation of k_{3-1} with $x_{1,3,5} = 0.01$ and $x_{2,4,6} = 0.04$ (panel 1: Oscillators; panel 2: Numerical results; column 3: Microcontroller results).

Declarations

Author contribution statement

Funding statement

Data availability statement

No data was used for the research described in the article.

Declaration of interest's statement

The authors declare no competing interests.

Additional information

No additional information is available for this paper.

References

[1] P. Pathmanathan, J.M. Cordeiro, R.A. Gray, Comprehensive uncertainty quantification and sensitivity analysis for cardiac action potential, Physiol. 10 (2019) 721.

[2] A. Cheffer, T.G. Ritto, M.A. Savi, Uncertainty analysis of heart dynamics using Random Matrix Theory, Int. J. Non LinearMech. 129 (2021), 103653.

[3] A. Brandão, M.A. Savi, Nonlinear mechanics of a smart biotensegrity human foot prosthesis, Int. J. Appl. Mech. 14 (1) (2022), 2150124.

[4] M.A. Quiroz-Juárez, O. Jiménez-Ramírez, R. Vázquez-Medina, V. Breña-Medina, J.L. Aragón, R.A. Barrio, Generation of ECG signals from a reaction diffusion model spatially discretized, Sci. Rep. 9 (2019) 1–10.

[5] L.L. Sala, M. Crestani, S. Garavelli, P. de Candia, A.E. Pontiroli, Does microRNA disruption control the mechanisms linking obesity and diabetes? Implications for cardiovascular risk, Int. J. Mol. Sci. 22 (1) (2021) 143.

[6] Y.T. van der Schouw, Y. van der Graaf, E.W. Steyerberg, M.J.C. Eijkemans, J.D. Banga, Age at menopause as a risk factor for cardiovascular mortality, Lancet 347 (1996) 714–718.

[7] A. Cheffer, M.A. Savi, Random effects inducing cardiac pathological dynamics: a mathematical model-based approach, Biosystems 196 (2020), 104177.

[8] B.B. Ferreira, M.A. Savi, A.S. De Paula, Chaos control applied to cardiac rhythms represented by ECG signals, Phys. Scripta 89 (2014), 105203.

[9] D. Baleanu, S. Sadat Sajjadi, J.H. Asad, A. Jajarmi, E. Estiri, 2021 Hyperchaotic behaviors, optimal control and synchronization of a non-autonomous cardiac conduction system, Adv. Differ. Equ. 157 (2022), 03320.

[10] M.C. De Almeida, S. Shumpei Mori, R.H. Anderson, Three-dimensional visualization of the bovine cardiac conduction system and surrounding structures compared with arrangements in the human heart, J. Anat. 238 (6) (2021) 1359–1370.

[11] S.N. Britin, M.A. Britina, R.Y. Vlasenko, Cardiac conduction system: a generalized electrical model, Biomed. Eng. 55 (2021) 41–45.

[12] K.M.V. Narayan, T.J. Thompson, J.P. Boyle, G.L.A. Beckles, M.M. Engelgau, F.V.D.F. Williamson, The use of population attributable risk to estimate the impact of prevention and early detection of type 2 diabetes on population-wide mortality risk in US males, Health Care Manag. Sci. 2 (1999) 223–227.

[13] E.D. Adrian, D.W. Bronk, G. Phillips, Discharges in mammalian sympathetic nerves, J. Physiol. 2 (1932) 115–133.

[14] S.R.F.S.M. Gois, M.A. Savi, An analysis of heart rhythm dynamics using a three-coupled oscillator model Chaos, Solitons Fractals 41 (2009) 2553–2565.

[15] D.S. Park, G.I. Fishman, The cardiac conduction system, Circulation 8 (2011) 904–915.

[16] A. Akgul, M.A. Savi, M.Z. Yildz, A.F. Miguel Sanjuan, J. Ma, Complex bio rhythms, Eur. Phys. J. Spec. Top. 231 (2022) 815–818.

[17] L. Glass, Introduction to controversial topics in nonlinear science: is the normal heart rate chaotic? Chaos 19 (2009), 028501.

[18] E. Ryzhii, M. Ryzhii, Modeling of heartbeat dynamics with a system of coupled nonlinear oscillators, in: Proceedings of the International Conference on Biomedical Informatics and Technology, Springer, Berlin, Heidelberg, 2013, pp. 67–75, 0.

[19] V.I. Krinsky, Mathematical models of cardiac arrhythmias (spiral waves), Pharmacol. Ther. 3 (1978) 539–555.

[20] G.J. Noordergraaf, J.T. Ottesen, W.J.P.M. Kortsmit, W.H.A. Schilders, G.J. Scheffer, A. Noordergraaf, The donders model of the circulation in normo- and pathophysiology, Cardiovasc. Eng. 6 (2006) 51–70.

[21] S. Nazari, A. Heydari, J. Khaligh, Modified modeling of the heart by applying nonlinear oscillators and designing an appropriate control signal, Appl. Math. 4 (2013) 972–978.

[22] R.M. Evaristo, A.M. Batista, L.R. Viana, K.C. Iarosz, J.J.D. Szezech, M.F. Godoy, Mathematical model with autoregressive process for eletrocardiograma signals, Commun. Nonlinear Sci. Numer. Simulat. 57 (2017) 415–421.

[23] B. Van der Pol, J. Van der Mark, The heartbeat as a negative resistance oscillator, and an electrical model of the heart, Phil. Mag. 7 (1928) 763–775.

[24] R. Tung, N.G. Boyle, K. Shivkumar, Catheter ablation of ventricular tachycardia, Circulation 122 (2010) e389–e391.

[25] K.C. Thies, K. Boos, K. Müller-Deile, W. Ohrdorf, T. Beushausen, P. Townsend, Ventricular flutter in a neonate–severe electrolyte imbalance caused by urinary tract infection in the presence of urinary tract malformation, J. Emerg. Med. 18 (1) (2000) 47–50.

[26] G. Giridharan, M. Skliar, Nonlinear controller for ventricular assist devices, Artif. Organs 26 (2002) 980–984.

[27] D.M. Sacknoff, G.W. Gleim, N. Stachenfeld, N.L. Coplan, Effect of athletic training on heart rate variability, Am. Heart J. 127 (1994) 1275–1278.

[28] D. Bernardo, D. Signorini, M. Gabriella, A. Cerutti Sergi, Model of two coupled nonlinear oscillators for the study of heartbeat dynamics, Int. J. Bifurc. Chaos 8 (1998) 1985, 1975.

[29] JiQian Zhang, Li Xiang, LiSi Liang, ShouFang Huang, HengGui Zhang, Effects of external stimuli on the pacemaker function of the sinoatrial node in sodium channel gene mutations models, Sci. China Life Sci. 56 (2013) 818–822.

[30] G.F. Romiti, D. Pastori, J.M. Rivera-Caravaca, W.Y. Ding, Y.X. Gue, D. Menichelli, J. Gumprecht, M. Koziel, P. Yang, Y. Guo, Y.H. Gregory Lip, M. Proietti, Adherence to the 'atrial fibrillation better care' pathway in patients with atrial fibrillation: impact on clinical outcomes-A systematic review and meta-analysis of 285,000 patients, Thromb. Haemostasis 122 (3) (2022) 406–414.

[31] T.F. Chao, B. Joung, Y. Takahashi, T.W. Lim, E.K. Choi, Y.H. Chan, Y. Guo, C. Sriratanasathavorn, S. Oh, K. Okumura, G.Y.H. Lip, 2021 focused update consensus guidelines of the asia pacific heart rhythm society on stroke prevention in atrial fibrillation: executive summary[*]. CC BY-NC-ND 4.0, Thromb. Haemostasis 122 (1) (2022) 20–47.

[32] H. Anthony Kashou, A. Demilade Adedinsewo, A. Peter Noseworthy, Subclinical atrial fibrillation: a silent threat with uncertain implications. Focused update consensus guidelines of the asia pacific heart rhythm society on stroke prevention in atrial fibrillation: executive summary [*]. CC BY-NC nd 4.0, Annu. Rev. Med. 73 (17) (2021) 355–362.

[33] V. Loen, A. Marc Vos, A.G. Marcel van der Heyden, The canine chronic atrioventricular block model in cardiovascular preclinical drug research, Br. J. Pharmacol. 179 (2021) 859–881.

[34] D. Alehan, C. Ayabakan, S. Özer, Heart rate variability and autonomic nervous system changes in children with vasovagal syncope, Pacing Clin. Electrophysiol. 25 (2003) 1331–1338.

[35] Aino-Maija Vuorinen, J. Lehtonen, S. Pakarinen, M. Holmström, S. Kivistö, T. Kaasalainen, Cardiac magnetic resonance imaging-based screening for cardiac sarcoidosis in patients with atrioventricular block requiring temporary pacing, J. Am. Heart Assoc. 11 (11) (2022), e02425.

[36] T.W. Hansen, Y. Li, J.A. Staessen, Blood pressure variability remains an elusive predictor of cardiovascular outcome, Am. J. Hypertens. 22 (2009) 3–4.

[37] Radu-Andrei Baz, C. Scheau, A. Constantin Rusali, P. Bordei, Computed tomography-assessed variations of the carotid sinus, Surg. Radiol. Anat. 44 (2022) 293–298.

[38] P. Pathmanathan, J.M. Cordeiro, R.A. Gray, Comprehensive uncertainty quantification and sensitivity analysis for cardiac action potential models, Front. Physiol. 10 (2019) 721.

[39] E. Ryzhii, M. Ryzhii, Heterogeneous coupled oscillator model for simulation of ECG signals, Comput. Methods Progr. Biomed. 117 (2014) 40–49.

[40] B. Van der Pol, J. Van der Mark, On relaxation-oscillations, Phil. Mag. 2 (1926) 978–992.

[41] R.F. Fonkou, P. Louodop, P.K. Talla, P. Woafo, Analysis of the dynamics of new models of nonlinear systems with state variable damping and elastic coefficients, Heliyon 8 (2022), e10112.

[42] C. Morris, H. Lecar, Voltage oscillations in the barnacle giant muscle fiber, J. Biophys. 35 (2021) 193–213.

[43] A.L. Hodgkin, A.F. Huxley, A quantitative description of membrane current and its applications to conduction and excitation in nerve, J. Physiol. 117 (1952) 500–544.

[44] R. FitzHugh, Impulses and physiological states in theoretical models of nerve membrane, Biophys. J. 1 (1961) 445–466.

[45] K. Grudzinski, J.J. Zebrowski, Modeling cardiac pacemakers with relaxation oscillators, Physica A 336 (2004) 153–162.

[46] R.F. Fonkou, Patrick Louodop, P.K. Talla, P. Woafo, Dynamic behaviour of pacemaker models subjected to a blood pressure excitation simulator: a theoretical and experimental study by microcontroller, Braz. J. Phys. 51 (2021) 1448–1458.

[47] R.F. Fonkou, P. Louodop, P.K. Talla, Nonlinear oscillators with variable state damping and elastic coefficients, Pramana - J. Phys. 95 (2021) 210.

[48] G. Krstacic, A. Krstacic, A. Smalcelj, D. Milicic, M. Jembrek-Gostovic, The chaos theory and nonlinear dynamics in heart rate variability analysis: does it work in short-time series in patients with coronary heart disease? Ann. Noninvasive Electrocardiol. 12 (2007) 130–136.

[49] J. Ernst, Z. Bar-Joseph, A tool for the analysis of short time series gene expression data, *BMC*.BMC Bioinform. 7 (2006) 1–11.

[50] D.P. Tobón, S. Jayaraman, T.H. Falk, Spectro-temporal electrocardiogram analysis for noise- robust heart rate and heart rate variability measurement, IEEE J. Transl. Eng. Health Med. 5 (2017) 1–11.

[51] Y. Shiraishi, Y. Katsumata, T. Sadahiro, K. Azuma, K. Akita, S. Isobe, F. Yashima, K. Miyamoto, T. Nishiyama, Y. Tamura, T. Kimura, N. Nishiyama, Y. Aizawa, K. Fukuda, S. Takatsuki, Real-time analysis of the heart rate variability during incremental exercise for the detection of the ventilatory threshold, J. Am. Heart Assoc. 7 (2018), e006612.

[52] M.A. Savi, Chaos and order in biomedical rhythms, J. Braz. Soc. Mech. Sci. Eng. 27 (2) (2015) 157–169.

[53] M.A. Savi, F.H.I. Pereira-Pinto, A.M. Ferreira, Chaos control in mechanical systems, Shock Vib. 13 (4/5) (2006) 301–314.

[54] G.C.G. Kuate, H.B. Fotsin, On the nonlinear dynamics of a cardiac electrical conduction system model: theoretical and experimental study, Phys. Scripta 97 (2022), 045205.

[55] A. Cheffer, M.A. Savi, T.L. Pereira, A.S. de Paula, Heart rhythm analysis using a nonlinear dynamics perspective, Appl. Math. Model. 96 (2021) 152–176.

[56] R.F. Fonkou, P. Louodop, P.K. Talla, Dynamic behaviour of the cardiac conduction system under external disturbances: simulation based on microcontroller technology, Phys. Scripta 97 (2022), 025001.

[57] W.H. Organisation Cardiovascular diseases (CVDs)(https://who.int/news-room/fact-sheets/detail/cardiovascular-diseases-(cvds)) (accessed December, 13, 2020).

[58] T. Fonzin Fozin, B. Koumetio Nzoko, N.A. Kengnou Telem, Z. Tabekoueng Njitacke, A.A. Ngo Mouelas, J. Kengne, Coexistence of hyperchaos with chaos and its control in a diode-bridge memristor based MLC circuit with experimental validation, Phys. Scripta 97 (2022) 075204.

[59] Z. Njitacke Tabekoueng, S.S. Muni, T. Fonzin Fozin, G.D. Leutcho, J. Awrejcewicz, Coexistence of infinitely many patterns and their control in heterogeneous coupled neurons through a multistable memristive synapse, Chaos 32 (2022), 053114.

[60] A. Wolf, J.B. Swift, H.L. Swinney, J.A. Vastano, Determining Lyapunov exponents from a time series, Phys. Nonlinear Phenom. 16 (1985) 285–317.

[61] W.J. Cunningham, A nonlinear differential-difference equation of growth, Proc. Natl. Acad. Sci. USA 40 (1954) 708–713.

[62] B.T. Davey, C. Quintana, S. Upadhyay, An unusual case of commotio cordis resulting in ventricular flutter, J. Emergencies, Trauma, Shock 11 (3) (2018) 225–227.

[63] A. Ricardo, M. Samson Vinay, Nadkarni, A. Peter Meaney, M. Scott Carey, D. Marc Berg, A. Robert Berg, Outcomes of in-hospital ventricular fibrillation in children, N. Engl. J. Med. 354 (2006) 2328–2339.

[64] M. Zoni-Berisso, F. Lercari, T. Carazza, S. Domenicucci, Epidemiology of atrial fibrillation, Clin. Epidemiol. 6 (2014) 213–220.

[65] E. Dimosthenis, A. Bolanakis, A survey of research in microcontroller education, IEEE Rev. Iberoam. Tecnol. Aprendiz. 14 (2) (2019) 50–57.

[66] R. Hasan, M.M. Khan, A. Ashek, I.J. Rumpa, Microcontroller based home security system with GSM technology, Open J. Saf. Sci. Technol. 5 (2) (2015) 7.

[67] X. Sun, W. Yuan, K. Jin, Y. Zhang, Control of the redox potential by microcontroller technology. Researching the leaching of chalcopyrite, Minerals 11 (4) (2021) 382.

[68] R.F. Fonkou, Patrick Louodop, P.K. Talla, P. Woafo, Van der Pol equation with sinusoidal nonlinearity: dynamic behaviour and real-time control of a target trajectory, Phys. Scripta 96 (2021), 125203.